Journal of Translational Medicine

RESEARCH

Open Access

Revolutionizing the treatment of intervertebral disc degeneration: an approach based on molecular typing

Shaofeng Chen[1,2†], Wei Zhang[3,4†], Yifan Liu[5,6†], Runzhi Huang[3,4*], Xiaoyi Zhou[1*] and Xianzhao Wei[1*]

Abstract

Background Intervertebral disc degeneration (IVDD) is a significant cause of global disability, reducing labor productivity, increasing the burden on public health, and affecting socio-economic well-being. Currently, there is a lack of recognized clinical approaches for molecular classification and precision therapy.

Methods Chondrocyte differentiation and prognosis-related genes were extracted from single-cell RNA sequencing and multi-omics data in the Gene Expression Omnibus (GEO) database through chondrocyte trajectory analysis and non-parametric tests. Subsequently, a precise IVDD risk stratification system was developed using ConsensusClusterPlus analysis. The clinical significance of molecular typing was demonstrated through case–control trials involving IVDD patients. Specific inhibitors of molecular typing were predicted using the pRRophetic package in R language and then validated in vitro.

Results A stratified model for IVDD, considering chondrocyte differentiation and demonstrating high clinical relevance, was developed using a set of 44 chondrocyte fate genes. Extensive analyses of multi-omics data confirmed the clinical relevance of this model, indicating that cases in the High Chondrocyte Scoring Classification (HCSC) group had the most favorable prognosis, whereas those in the Low Chondrocyte Scoring Classification (LCSC) group had the worst prognosis. Additionally, clinical case–control studies provided evidence of the utility of IVDD molecular typing in translational medicine. A gene expression-based molecular typing approach was used to create a matrix identifying potential inhibitors specific to each IVDD subtype. In vitro experiments revealed that gefitinib, a drug designed for LCSC, not only had protective effects on chondrocytes but also could induce the conversion of LCSC into the HCSC subgroup. Therefore, IVDD molecular typing played a critical role in assisting clinicians with risk stratification and enabling personalized treatment decisions.

Conclusion The results of the study have provided a comprehensive and clinically relevant molecular typing for IVDD, involving a precise stratification system that offers a new opportunity for customizing personalized treatments for IVDD.

Keywords IVDD, Single-cell RNA sequencing, Molecular subtype, Case–control trial, Gefitinib

†Shaofeng Chen, Wei Zhang, and Yifan Liu have contributed equally to this work.

*Correspondence:
Runzhi Huang
runzhihuang2022@163.com
Xiaoyi Zhou
13818909826@163.com
Xianzhao Wei
weixianzhao@126.com
Full list of author information is available at the end of the article

Background

The prevalence of disc degenerative diseases (DDD) has increased progressively due to the aging population, becoming a major contributing factor to global disability [1–4]. The degenerative process starts with intervertebral disc degeneration (IVDD), causing structural and functional impairments [5–7]. IVDD-induced lower back pain (LBP) has persistently affected around 80 percent of adults [8]. In the 2010 Global Burden of Disease study, LBP ranked highest in disability among the 291 diseases examined [9]. Furthermore, it significantly contributed to the reduction in global labor productivity, thereby increasing the burden on public health resources and reducing socio-economic well-being [10].

The goal of treating IVDD is to relieve symptoms and improve the quality of life for individuals affected by the condition [11]. This is accomplished through various approaches, such as conservative measures like lumbar muscle exercises, as well as physical and pharmacological interventions [12]. Additionally, disc repair therapies involving genes [13], cells [14], and growth factors [15], along with decompression surgery [16–18], are employed. Nevertheless, it is important to note that numerous intervertebral disc repair therapies remain in the experimental or clinical trial phase due to the current medical knowledge and understanding of IVDD. Currently, IVDD has relied on conservative and surgical interventions in clinical practice, exhibiting a dichotomous pattern [11]. However, both approaches possess inherent limitations. Conservative treatment is primarily applicable to patients with mild degeneration, while the administration of opioids and non-steroidal drugs may lead to addiction and patient dependency [19]. Furthermore, the utilization of total intervertebral disc replacement surgery is commonly advised for patients presenting with single-segment lesions and the absence of minor joint lesions [20]. Nevertheless, it is crucial to acknowledge that decompression and fusion surgery, which entails sacrificing spinal segmental movement, is linked to numerous complications and substantial expenses. Moreover, an estimated 30% of patients may encounter persistent or recurring LBP subsequent to the surgical procedure [21–23].

As a result, the absence of a clinically viable protocol for personalized diagnosis and treatment of IVDD and the dearth of clinically acknowledged strategies for molecular typing and precision diagnosis and treatment of IVDD are evident. Consequently, there is a need for tools that can effectively differentiate the severity of the disease, precisely ascertain disease prognosis, and aid clinicians in risk stratification and treatment decision-making for patients afflicted with IVDD, in order to optimize the diagnostic and treatment system.

The intervertebral disc, referred to as the intervertebral fibrocartilage disc, is primarily comprised of a substantial quantity of fibrocartilage [24, 25]. In terms of its structure, it assumes a flat, disk-shaped form, encompassing end-plate cartilage and a fibrous annulus that encloses the nucleus pulposus tissue. The cartilage tissues and cells serve a dual purpose of stress dispersion and facilitating the transportation of nutrients and metabolites [26]. Furthermore, recent research has indicated the significance of chondrocyte metabolism in the advancement of IVDD [27, 28].

In this study, we acquired a dataset consisting of single cell sequencing data of intervertebral disc fibroring tissue cells and clinical information from patients diagnosed with IVDD, obtained from a publicly available database. A total of 25,974 chondrocytes were extracted from the single cell sequencing data for pseudotime analysis, resulting in the identification of 1,058 chondrocyte differentiation-related genes (CDGs). Additionally, genes linked to the severity of degeneration and Thompson grading were extracted from IVDD microarray data. Furthermore, by intersecting these genes with the aforementioned ones, we obtained a set of 44 chondrocyte differentiation and prognosis related genes (CDPRGs). Using CDPRGs as a basis, we developed a molecular typing model for IVDD with three distinct classifications. This was achieved through the application of the ConensusClusterPlus algorithm and principal component analysis (PCA). Subsequently, we conducted a comprehensive analysis of multi-omics data and employed non-parametric tests to investigate the clinical relevance and predictive value of this classification. Furthermore, we have successfully identified distinct marker genes for each of the three subtypes by analyzing their relative expression levels of CDPRGs. Subsequently, we have conducted clinical case–control studies to investigate the potential clinical applicability of these subtypes. Additionally, we have screened various drugs that exhibit differential sensitivity based on the expression patterns of the three subtypes, and further validated their efficacy through in vitro experiments. In summary, our study has put forth a molecular typing method for IVDD based on chondrocyte differentiation. The objective of this approach was to facilitate the categorization of risk and evaluation of prognosis in patients with IVDD, while also validating its clinical translational utility and presenting potential avenues for therapy.

Materials and methods

Collection of public data: ethics statement

The Ethics Committee of Shanghai Changhai Hospital has granted approval for the protocol of this study, as indicated by the Ethics Approval Document No. CHEC2022-262. The Gene Expression Omnibus (GEO) database was utilized to obtain single-cell sequencing data for two annulus fibrosus (AF) samples (GEO accession: GSE160756) (https://www.ncbi.nlm.nih.gov/geo/query/acc.cgi?acc=GSE160756) [29]. Furthermore, we obtained the pertinent data of 38 microarrays from patients with IVDD and their corresponding clinical information from the GEO database, as depicted in Table S1. (GEO accession: GSE15227 and GSE23130) (https://www.ncbi.nlm.nih.gov/geo/query/acc.cgi?acc=GSE15227) [30] and (https://www.ncbi.nlm.nih.gov/geo/query/acc.cgi?acc=GSE23130) [31].

Data processing and visualization

The 10×Genomics Chromium program (https://www.10xgenomics.com/instruments/chromium-x-series) [32] was utilized to preprocess single cell RNA sequencing (scRNA-seq) data. Initially, a fastq file was created from the raw scRNA-seq data through the employment of the cellranger mkfastq command within the Cell Ranger package (v3.0, http://10xgenomics.com/). Subsequently, the fastq file underwent pruning to eliminate the template switch oligonucleotide sequence and the polyA tail sequence. Following this, a comparison was made between the pruned fastq file and the human reference genome (version: Ensemble GRCh38), and the gene expression matrix was computed using the Cell Ranger counting software. The affy package was employed for microarray data analysis, wherein Robust Multi-array Average (RMA) background correction and data standardization techniques were applied [33]. Subsequently, probe sequences were annotated, resulting in the acquisition of gene expression matrices for all samples [34]. Furthermore, the sva software package was utilized to perform necessary batch corrections [35].

In the context of downstream visualization analysis, an initial step of quality control (QC) was conducted to identify cells exhibiting transcript expression exceeding 100,000 and mitochondrial gene localization below 10%. These cells were selected for further analysis, wherein the inclusion criteria encompassed the presence of two or more expressed genes per individual cell. Following the completion of the aforementioned QC process, the gene expression matrices of the all samples were integrated into a Seurat object using the "IntegrateData" function. Subsequently, the "ScaleData" function was employed to normalize the integrated gene expression matrix. The "vst" method was employed to identify the initial set of 2,000 highly variant genes. To reduce dimensions, PCA was initially applied, and the first 20 significant principal components (PCs) were integrated into a Uniform Manifold Approximation and Projection for Dimension Reduction (UMAP) algorithm to obtain a representation of the overall cell population. Subsequently, a gene was classified as a differential expression gene (DEG) if it met the criteria of $|\log2 \text{ Fold Change (FC)}| > 0.5$ and a False Discovery Rate (FDR) < 0.05. Subsequently, we employed the "FindAllMarkers" function and the Wilcoxon rank sum test to scrutinize DEGs within the top 2,000 highly variable genes. This analysis aimed to discern the gene expression patterns of cell markers, facilitating the labeling of distinct cell types.

Cell type annotation

In order to ascertain the cell types present in each unsupervised cluster, DEGs were utilized as potential references in all subclusters. This approach was combined with the incorporation of specific cell surface biomarkers known in CellMarker, resulting in a comprehensive annotation of cell types [36]. The identified cell types in the known AF tissues encompassed chondrocytes (*c2orf40, fgfbp2, serpina1*), stromal cells (*apoe, marcks, hes4*), blood cells (*hla-dra, ccl3, fcer1g*), peripheral cells (*tagln, rgs5, sparcl1*), myelonuclear progenitor cells (*dpp4, nox4, vit*), and endothelial cells (*ifi27, sparcl1, cd74*). Furthermore, the generation of cell signature maps, Cleveland point maps, and heat maps was accomplished utilizing Seurat (Version: 3.2.2) within the R package and SCANPY (Version: 1.7.1) in Python 3.6 to visually represent annotated genes specific to each cell type [36, 37]. Moreover, chondrocytes were instantiated as a Seurat object in all samples. Subsequently, employing the aforementioned methodology, distinct cell subtypes within chondrocytes were identified, and the top five DEGs of highly mutated genes were elucidated using Cleveland point and heat maps.

Cellular communication analysis

To investigate the patterns of cellular communication and identify the precise ligand-receptor pairs, we conducted an integrated cellular communication analysis using the iTALK package (Version: 0.1.0) in the R programming language [38]. Initially, the expression matrix of the genes under study was standardized, and the standardized expression matrix was inputted into the iTALK analysis via the "rawParse" function [39]. Subsequently, the corresponding relationships between ligands and receptors in cellular communication were obtained through the built-in database (https://github.com/Coolgenome/iTALK). Thereafter, the Wilcoxon rank-sum test was employed to determine the cellular communication

patterns with significant differences among various cell types. The top 200 cellular communication patterns with the smallest P-values were selected. Through the utilization of ligand-receptor plots and the iTALK network, in conjunction with the edge bundle R package (https://github.com/garthtarr/edgebundleR), the visualization of the top 200 ligand-receptor pairs was accomplished.

Construction of chondrocyte differentiation trajectory

The analysis of chondrocyte differentiation trajectory was conducted using the Monocle software package (Version: 2.18.0) [40]. The objective of this analysis was to elucidate the translation relationships among various subtypes of chondrocytes. The determination of chondrocyte differentiation order relied on comparing expression profiles and matching pseudotime associated with individual chondrocyte subtypes. The "reduceDimension" function of DDRTress was employed to ascertain the pseudotime of distinct chondrocyte subpopulations and to visually represent the ensuing outcomes via a trajectory map [40]. The differentiation trajectories were subsequently sequenced, computed, and scrutinized for DEGs, denoted as CDGs, according to the criterion of meeting the q value < 0.05 in the DDRTress algorithm.

ConsensusClusterPlus analysis

Before the implementation of the Chondrocyte Differentiation Based IVDD Classification (CDBIVDDC), CDPRGs were screened through non-parametric testing and Venn diagrams. Subsequently, CDBIVDDCs were developed utilizing the identified CDPRGs. ConsensusClusterPlus software was employed to achieve consistent clustering, whereby samples exhibiting similar attributes were grouped together.

PCA and clinical prognostic parameters of IVDD

Chondrocyte scores were determined for each sample by employing the PCA algorithm to analyze the expression patterns of CDPRGs [41]. Simultaneously, the relationship between chondrocyte differentiation and IVDD prognosis was investigated, and the clinical significance and potential utility of clinical transformation of CDBIVDDC were assessed. CDBIVDDC was utilized as a classification variable, while chondrocyte score served as a continuous variable for comparison with the degree of disc degeneration and Thompson grade of patients. The results were visually represented through box plots and bar plots, with statistical significance indicated by a two-sided *P*-value < 0.05.

The aging process is associated with various levels of degeneration in the intervertebral disc, resulting in alterations such as fibrous ring degeneration, swelling, dehydration, stiffness, and fissure formation. These changes progressively contribute to spinal instability, bone-fold formation, intervertebral disc protrusion, spinal canal stenosis, ligament ossification, and subsequent irritation or compression of nerves, leading to the emergence of corresponding clinical symptoms [42]. A comprehensive understanding of the degree of disc degeneration is crucial for clinicians to gain insights into the patient's condition. The database provides valuable information regarding the symptoms and prognosis of IVDD, primarily assessed through the Thompson grade [43], which effectively captures the morphological alterations and pathological advancement of the disc components. In line with prior research [31], we have categorized Thompson grades I to III as representing Less Degeneration (LD), while grades IV to V are classified as More Degeneration (MD) (Table S1).

Collection of patients with IVDD

In this study, samples of intervertebral disc were obtained from patients who were diagnosed with IVDD and underwent lumbar disc removal fusion surgery at the Department of Spinal Surgery of Shanghai Changhai Hospital between March 1, 2022, and June 1, 2023. The collected intervertebral disc samples were processed into paraffin specimens to be utilized for subsequent Immunohistochemistry (IHC) analysis. The study population was selected based on specific inclusion criteria, which included individuals who were 18 years or older, had an educational background of junior high school level or higher, were diagnosed with IVDD, met the indications for discectomy and fusion, had comprehensive preoperative imaging and clinical information, exhibited a complete preoperative function score on the Oswestry Disability Index (ODI) scale, and expressed willingness to participate in the study. The exclusion criteria comprised a range of factors, such as previous spinal fractures, malformations, infections, tumors, congenital developmental abnormalities, spinal cord injuries, spinal cavities, spinal cord concussion injuries, and other diseases. Furthermore, participants were excluded if they had incomplete data regarding preoperative imaging from the Changhai Hospital PACS imaging system or other clinical information, lacked functional scales or displayed irregularities, or had a background of severe chronic systemic diseases.

Patient demographics, including numbers, age, sex, occupation, smoking history, adjacent segment degenerative disease, patient lumbar MRI Pfirrmann grade [44], and ODI scale scores, were systematically collected and documented. The assessment of the Pfirrmann grade was conducted independently by two spine surgeons, and their findings were ultimately consolidated. In cases of disagreement, a senior associate professor specializing in spine surgery provided final judgment and assessment.

The collection process adheres rigorously to the Standards for Reporting of Diagnostic Accuracy Studies Statement and the Strengthening the Reporting of Observational Studies in Epidemiology (STROBE) guidelines.

IHC staining and scoring

The 4 μm paraffin sections of human intervertebral disc tissue were subjected to dewaxing using water, citric acid antigen repair solution (pH 6.0), or EDTA antigen repair buffer (pH 9.0) for antigen repair. Subsequently, the sections were treated with 5% bovine serum albumin at room temperature for 30 min, followed by overnight incubation at 4°C with the first antibody and subsequent incubation at room temperature with the second antibody for 1 h the next day. Color development was achieved using DAB developing solution, resulting in the desired brown-yellow color observed under the microscope. The nucleus was restained with hematoxylin. The primary antibodies utilized in the dyeing procedure were as follows: adenylate cyclase activating polypeptide 1 (ADCYAP1) (ab181205, 1:200, abcam, USA); parathyroid hormone like hormone (PTHLH) (A1654, 1:100, abclonal, China); melanoma inhibitory activity (MIA) (LDQB-A2-21,331, 1:100, Leda, China); tubulin alpha 1c (TUBA1C) (ab222849, 1:50, abcam, USA); galectin-1 (LGALS1) (ab138513, 1:200, abcam, USA), anterior gradient homologous protein-2 (anterior gradient 2, AGR2) (ab76473, 1:100, abcam, USA). The evaluation of staining for each film was conducted by two pathology experts, who independently assessed the staining intensity and the percentage of positive staining cells. The final score was determined by multiplying the staining intensity with the percentage of positive staining cells. In the event of any inconsistencies in the scoring, a senior pathologist will be consulted for reassessment.

Cell culture

Human immortalized chondrocytes were procured from China Kuisai Biotechnology Co., LTD., and subsequently cultivated in a 5% CO_2 thermostatic (37 ℃) incubator using the complete culture medium specifically designed for immortalized chondrocytes (Kuisai Biotechnology Co., LTD., China). To establish a model of chondrocyte degeneration, chondrocytes were stimulated with 10 ng/ml IL-1β (Nearshore Protein Technology Co., LTD., China) for a duration of 24 h [45]. The cell experiment groups are as follows: control (Ctrl: cells cultured under normal conditions), IL-1β (cells stimulated with 10ng/ml IL-1β for 24 h), and IL-1β + Gefitinib (Absin Bioscience Co., LTD., China) (cells stimulated with 10 ng/ml IL-1β for 24 h, and then intervened with10 μM gefitinib for 48 h).

Cell Counting Kit-8 (CCK-8) assay

Human immortalized chondrocytes were seeded into 96-well plates at a density of 5×10^4 cells/ml with 100 ul per well, and subsequently cultured under suitable conditions as per the experimental protocol. 100 ul of medium containing 10% CCK-8 reagent (Dojindo, Japan) was introduced to each well and incubated in a constant temperature incubator for a duration of 2 h at 0, 24, 48 h. The absorbance at 450 nm was then quantified using a multifunctional enzyme marker.

Toluidine blue staining

Human immortalized chondrocytes were seeded at a density of 1×10^5 cells/ml and 1ml per well in 6-well plates, and subsequently cultured under suitable conditions as per the experimental protocol. Upon reaching a cell fusion degree of 80–90%, the cells were fixed using a 4% paraformaldehyde solution, followed by staining with toluidine blue solution (Solebol, China) for a duration of 30 min. The excess dye was then removed by washing with PBS buffer solution. Upon microscopic examination and photography, the nucleus exhibited a dark blue coloration, while the cytoplasm appeared blue.

RNA extraction and quantitative reverse transcription polymerase chain reaction (qPCR)

Total RNA was extracted through the application of Trizol reagent (15,596,026, Invitrogen, USA). Subsequently, reverse transcription was conducted utilizing the 036A kit (TaKaRa, Japan) as per the provided instructions. qPCR was carried out by means of the StepOnePlus real-time PCR system (Applied Biosystems, USA), in tandem with the RR820A kit (TaKaRa, Japan), with scrupulous compliance to the provided guidelines. The internal reference gene, beta-actin, was selected for normalization purposes. In this study, the primers were designed using the Primer Blast, a primer alignment tool provided by the National Center for Biotechnology Information (NCBI) (https://www.ncbi.nlm.nih.gov/tools/primer-blast/) [46]. The primer sequences and their corresponding targeted genes have been comprehensively and detailedly listed in Table S2.

Protein extraction and Western Blot

Total protein was extracted by RIPA lysate (P0013B, Biyuntian, China) supplemented with protease and phosphoprotease inhibitor (P002, Neosemet, China). The BCA protein concentration assay kit (P0011, Biyuntian, China) was utilized to determine the concentration of total protein. Subsequently, 10 μg protein samples were applied to the Omni-PAGETM prefabricated adhesive Hepes (LK202, Yatase, China) for gel electrophoresis,

followed by transfer onto a PVDF membrane. The non-specific binding sites were obstructed using a 5% skim milk solution, followed by an overnight incubation at 4 °C with the primary antibody. The subsequent day, the sample was incubated at room temperature for 2 h with the secondary antibody and subsequently visualized using an enhanced chemiluminescence (ECL). The primary antibodies utilized in this research encompassed GAPDH (AT0002, 1/1000, Engibody, USA); collagen type II (COL2) antibody (28,459–1-AP, 1/1000, Proteintech, China), SRY-box transcription factor 9 (SOX9) antibody (67,439–1-Ig, 1/1000; Proteintech, China), matrix metallopeptidase 13 (MMP13) antibody (18,165–1-AP, 1/2000, Proteintech, China), ADCYAP1 antibody (ab181205, 1/2000; abcam, USA) MIA antibody (ab186731, 1/1000; abcam, USA), employing secondary antibodies comprising horseradish peroxidase (HRP) labeled Goat anti-mouse IgG (LF101, 1/2000; Epizyme, China) and Goat Anti-Rabbit IgG (LF102, 1/2000; Epizyme, China).

Statistical analysis

In this study, statistical significance was determined based on double-tailed *P*-values < 0.05 and FDR < 0.05. The software R Version 4.0.3 (Institute of Statistics and Mathematics, Vienna, Austria; www.r-project.org), Python Version 3.6 (https://www.python.org/), and Strawberry Perl Version 5.30.0.1 (https://www.perl.org/) were employed for the statistical analysis process. Descriptive statistics for measurement data, such as normal distribution and homogeneity of variance, were obtained using the mean ± standard deviation. To compare between groups, either the independent sample t-test or ANOVA was employed. In cases where the measurement data did not adhere to a normal distribution, it was represented by M (P25, P75), and the comparison between groups was conducted using the Wilcoxon rank sum test or Kruskal–Wallis test. The counting data were expressed as frequency (percentage), and the Chi-square test was utilized for group comparisons.

Results

Cell type annotation

After undergoing rigorous screening and QC procedures, a total of 27,001 cells that satisfied the QC requirements were obtained from the scRNA-seq composite data of two AF samples. The general outline of this study was shown in the flowcharts of Fig. 1A and Figure S1. Subsequently, an unsupervised UMAP clustering analysis was conducted, resulting in the accurate identification of six unsupervised clusters and six distinct cell types, namely blood cells, chondrocytes, endothelial cells, nucleus pulposus progenitor cell (NPPC), pericytes, and stromal cells (Fig. 1B, C). A bar plot was employed to visually depict the quantity and proportion of each cell type, as shown in Fig. 1D. The results of Fig. 1D indicated that chondrocytes exhibited a significantly higher abundance and proportion compared to other cell types. Furthermore, the distribution of the aforementioned cell types was demonstrated by utilizing cell type-specific marker genes from the CellMarker database (Fig. 1E). Subsequently, a comprehensive analysis incorporating typical marker genes and clustering outcomes resulted in the identification and extraction of a total of 25,974 chondrocytes for subsequent investigations.

Comprehensive analysis of DEG, cell communication, and cell cycle for each subpopulation.

The top 2,000 hypervariable genes in the sample were subjected to DEG analysis, utilizing the six previously identified cell types. Cleveland dot plots and bar plots were employed to visually represent the expression of the classically labeled genes, as well as the various cell ratios (Figure S2A). As shown in the Figure S2A, *sox9* is highly expressed in chondrocytes. As a dominant transcription factor during chondrogenesis, *sox9* plays an important role in the genesis, growth and maturation of chondrocytes [47, 48]. Notably, chondrocytes constituted approximately half of each sample, indicating their predominant presence in the study samples. Furthermore, the heatmap provided detailed elucidation of the expression levels of the top 5 labeled DEGs (Figure S2B). In addition, the explication of intercellular communication networks and ligand-receptor maps provided valuable insights into the intricate mechanisms underlying intercellular signal transduction (Figure S2C, D). These findings highlighted the robust intercellular communication observed among diverse cell types. Simultaneously, we carried out a further screening to identify the genes with

(See figure on next page.)

Fig. 1 The comprehensive analysis of Single-cell RNA sequencing (scRNA-seq). **A** The image serves to emphasize a crucial stage in the workflow. **B** Through the utilization of UMAP dimensionality reduction analysis, a total of six distinct clusters were successfully identified from a population of 27,001 individual cells. **C** A compilation of six distinct cell types, namely Blood cell, Chondrocyte, Endothelial cell, NPPC, Pericyte, and Stromal cell, was acquired via the process of dimension reduction analysis. **D** The bar plot visually represented the quantity and proportion of individual cell types within all clusters. **E** The feature plots exhibited the distribution and expression levels linked to representative cell type markers, as documented in the CellMarker database

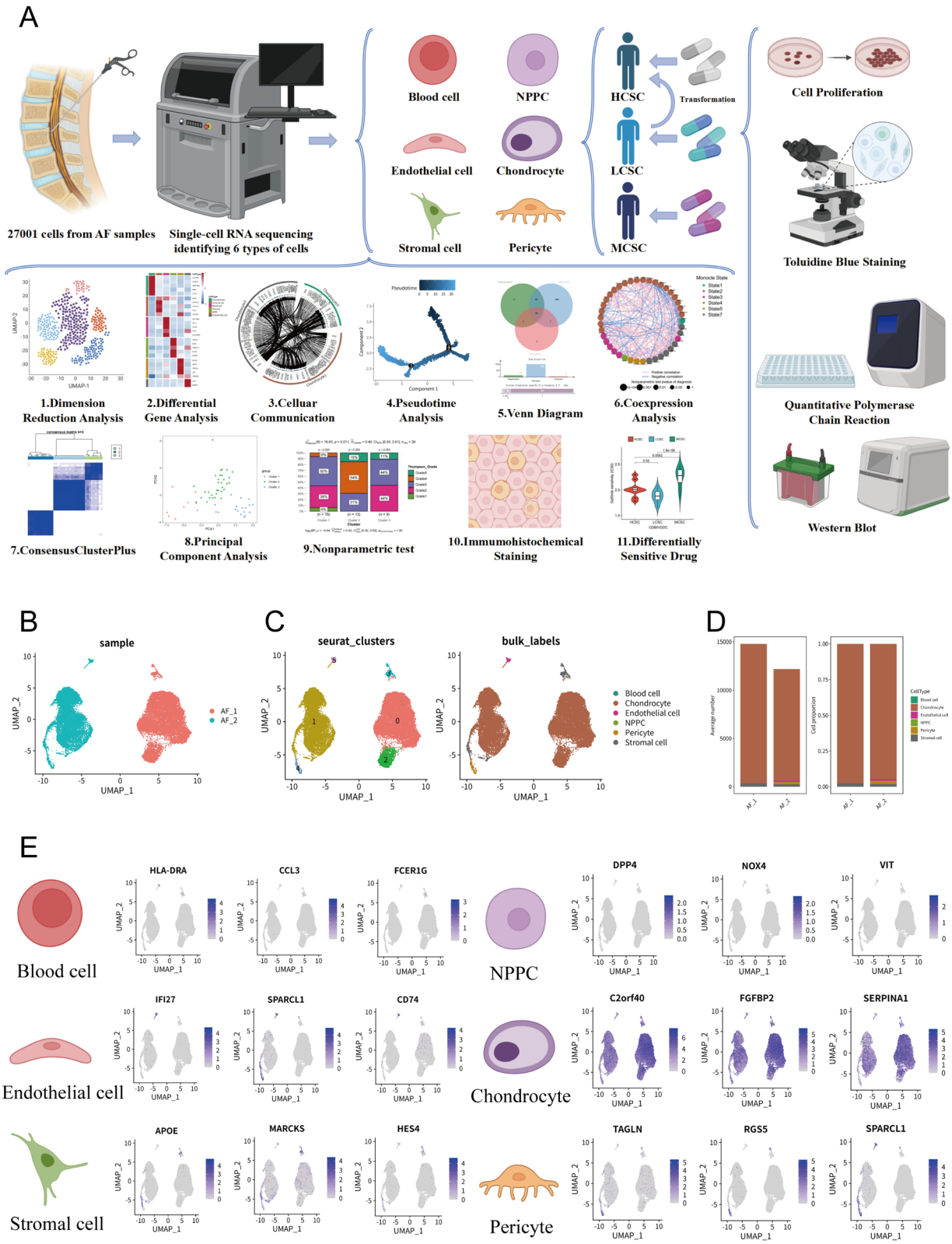

Fig. 1 (See legend on previous page.)

chondrocytes acting as both ligands and receptors, followed by a functional enrichment analysis. The findings indicated that the uPAR pathway is potentially implicated in the inflammatory response of chondrocytes [49]. The Integrin cell surface interactions play a role in mediating the interaction between chondrocytes and the extracellular matrix (ECM), exerting a significant biological function in maintaining the homeostasis and facilitating the repair of chondrocytes [50]. In contrast, the ECM-receptor interaction and ECM organization are likely to be associated with the progression of IVDD [51] (Figure S2E). Additionally, Figure S2 F, G presented the results of cell cycle analysis conducted on the aforementioned cells.

Characterization of chondrocyte lineage

The aforementioned analysis involved the extraction and construction of Seurat objects for each of the 25,974 chondrocytes. Initially, these chondrocytes were subjected to UMAP dimensionality reduction analysis, resulting in their clustering and subsequent annotation with cell subtypes. From this annotation, three major cell subsets were identified (Fig. 2A, B). Furthermore, the expression of classically labeled genes within different chondrocyte subtypes was visualized using Cleveland dot plots, while the proportions of the three chondrocyte subtypes were depicted through bar plots (Fig. 2C). Among them, type II collagen gene (*col2a1*), a cartilage-specific matrix protein, is actively involved in cartilage anabolic processes and, thus, plays a crucial part in maintaining cartilage homeostasis [52–54]. Likewise, chondroadherin (*chad*), a class IV small leucine-rich proteoglycan/protein, exhibits a close association with chondrocyte signal transduction [55, 56]. Moreover, cluster of differentiation 44 (*cd44*), a transmembrane glycoprotein on chondrocytes, acts as a communication bridge between the ECM and chondrocytes [57, 58]. In addition, marker of proliferation Ki-67 (*mki67*) plays a significant role in cell proliferation [59, 60]. Our observations revealed elevated expression of *chad* in both chondrocyte subtype 1 and chondrocyte subtype 3, heightened expression of *col2a1* exclusively in chondrocyte subtype 2, and diminished expression of *mki67* and *cd44* across all subpopulations. Heatmaps were subsequently employed to elucidate the expression levels of the five most prominently labeled DEGs within the three distinct chondrocyte subpopulations (Fig. 2D). Subsequently, the identification of potential ligand-receptor pairs within each chondrocyte subpopulation was conducted through the utilization of iTALK cell communication analysis. The outcomes were then visually represented by intersected cellular communication network and ligand-receptor plots (Fig. 2E, F).

Analysis of chondrocyte differentiation trajectory and identification of differentiation-related genes

To systematically model the fate decisions and gene expression dynamics of chondrocyte differentiation, Monocle2 was utilized to examine the differentiation trajectory of chondrocytes. By comparing the pseudotime of each chondrocyte subtype, the sequential order of differentiation for the 3 chondrocyte subpopulations was confirmed. The differentiation trajectory analysis results were presented in Fig. 3A–C and Figure S3A, B. Notably, the pseudotime-based chondrocyte differentiation trajectory revealed that chondrocytes could attain various cell fates starting from point 1. Figure 3A visually depicted the presence of branch points 1, 2, and 3, which resulted in the division of these cells into a total of 7 distinct future cellular states. In Fig. 3B, the chondrocyte differentiation pseudotime sequence was shown. A rise in the pseudotime value likely mirrors the increasing maturity of cell differentiation. Furthermore, Fig. 3C presented the distribution of chondrocyte clusters along the differentiation trajectory. Based on the result of pseudotime analysis, chondrocyte 3 (cluster 2) was predominantly situated in state 1, which aligned with the initiation point of the pseudotime trajectory, suggesting the potential possession of stem cell-like characteristics. Chondrocyte 1 (cluster 0) was chiefly found in states 1 through 5, corresponding to a position closer to the starting point within the intermediate section of the pseudotime. In contrast, chondrocyte 2 (cluster 1) was mainly distributed across states 5, 6, and 7, corresponding to a location nearer to the terminal part of the pseudotime, implying a relatively more mature stage of differentiation.

(See figure on next page.)

Fig. 2 Chondrocyte cluster identification and cellular communication analysis. **A** Chondrocyte clusters were identified using UMAP analysis of unsupervised clustering. **B** The UMAP plot depicted the spatial distribution of chondrocytes across various samples. **C** The Cleveland's dot plot represented the expression levels of four canonical marker genes associated with chondrocytes, while the stacked bar plot provided an indication of the quantity of chondrocyte clusters across various samples. **D** The heat map depicted the levels of gene expression for the top five marker genes within three distinct chondrocyte clusters. **E** The UMAP iTalk network analysis unveiled the presence of overlapping cellular communication within three distinct chondrocyte clusters. **F** The UMAP ligand-receptor plot elucidated the cellular communication mechanisms exhibited by three distinct clusters of chondrocytes, along with the identification of the genes accountable for facilitating this communication

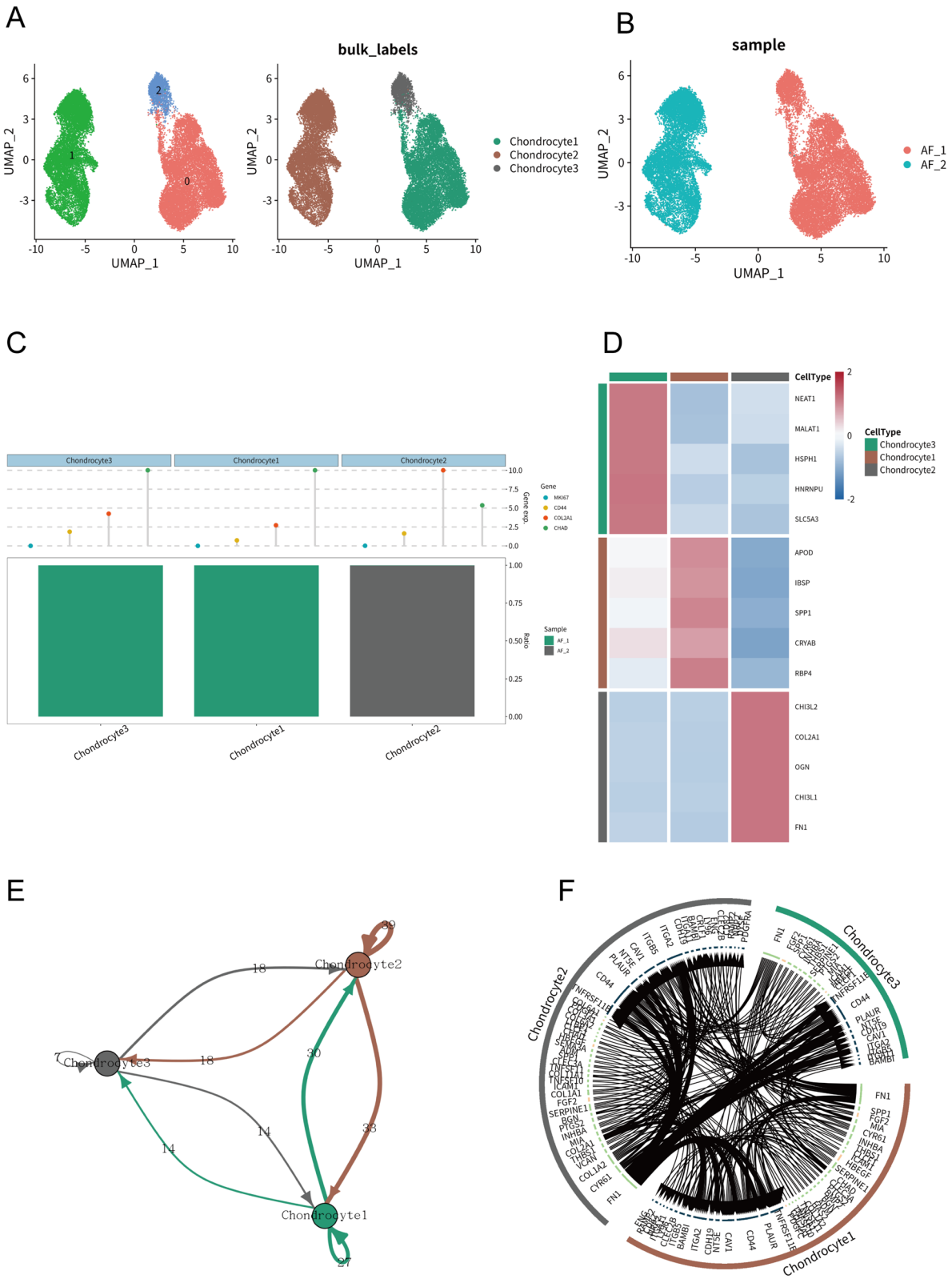

Fig. 2 (See legend on previous page.)

The identification of key genes played a crucial role in determining cell fate specification, exerting a significant influence on this process. Consequently, branch point 1 was designated as the cut-off point, and a comparative analysis of DEGs was conducted to examine the two primary branches representing cell fate 1 and cell fate 2. The resulting expression levels of genes in the seven cell state components were visually represented through a heat map (Fig. 3D), providing valuable insights into the direction of cellular differentiation. To provide further clarification, clusters 1, 3, 6, and 7 exhibited pronounced propensities for cell fate 1 differentiation. Conversely, clusters 2 and 5 displayed notable tendencies towards cell fate 2 differentiation. Additionally, no discernible disparity in differentiation tendencies for cell fate 1 and 2 was observed in cluster 4.

In order to investigate the sequential dynamics of gene expression in each branch, we conducted an analysis of DEGs and utilized Monocle2 trajectory analysis. The resulting findings were presented in a heat map (Fig. 3E), which depicted the expression levels of the top 100 genes associated with cell fate. Moreover, based on the scRNA-seq analysis, it could be inferred that these identified differentially expressed genes played a crucial role in all stages of cell differentiation (Figure S3C–E). We noted an elevated expression of podoplanin (*pdpn*), proline-rich nuclear receptor coactivator 2 (*pnrc2*), and stathmin 1 (*stmn1*) during the early stage. *Pdpn* expression correlates with the inflammatory response and contributes to the degeneration of chondroid structures [61, 62]. *Pnrc2* likely functions in mRNA degradation [63]. *Stmn1* is involved in chondrocyte differentiation; specifically, the mRNA and protein levels of *stmn1* in relatively immature chondrocytes are about twice those in growth zone chondrocytes, with a decreasing trend as differentiation progresses [64]. Additionally, alpha-enolase (eno1) and phospholipase A2, group IIA (*pla2g2a*) were markedly overexpressed at the late stage. *Eno1* activates the chondrocyte inflammatory pathway and is crucial for inflammation, apoptosis, and matrix degradation [65], while *pla2g2a* is linked to IVDD progression [66, 67]. Notably, as depicted in Figure S3C–E, heparan sulfate proteoglycan 2 (*hspg2*) exhibited a consistently low expression throughout. Research indicates that *hspg2* safeguards chondroid structures by modifying ECM characteristics, thereby remodeling tissue properties and functions [68].

Integration of chondrocyte differentiation and prognosis-related genes

To enhance the comprehension of gene expression during various phases of chondrocyte differentiation, a total of 1058 genes were identified using the DDRTress algorithm. These genes met the criterion of $q < 0.05$ and were associated with the differentiation trajectory of chondrocyte subpopulations, referred to as CDGs. Using the 1,058 CDGs identified in the aforementioned analysis, along with the gene expression profiles and clinical information available in the GEO database, a single-factor regression analysis was conducted. This analysis aimed to identify genes significantly associated with degeneration ($P < 0.001$) and Thompson grading (Thompson-significant; $P < 0.001$). The intersection of these analyses, represented by the Venn diagram, yielded a total of 44 genes (Figure S4A and Table S3). These genes, referred to as CDPRGs, were utilized in the subsequent construction of IVDD molecular typing. In addition, to verify the reliability of CDPRGs, we further conducted external validation through scRNA-seq data from public databases. Table S4 showed the sample information of the scRNA-seq data. Figure S5A, B and Figure S6 presented the feature plots of CDPRGs and their expression levels in healthy volunteer (HV) and patients with IVDD.

Furthermore, boxplots were employed to visually represent the outcomes of clinical correlation analysis conducted on the CDPRGs in relation to the severity of IVDD and Thompson grade (Figure S4B). In particular, we were concerned about the significant association between the expression levels of the *adcyap1* and *pthlh* genes and a reduced degree of degeneration and lower Thompson grades ($P < 0.001$). Conversely, the expression levels of the *mia* and *tuba1c* genes were significantly associated with an increased degree of degeneration and higher Thompson grades ($P < 0.001$).

(See figure on next page.)

Fig. 3 Chondrocyte developmental pathway and fate-related genes were revealed using Monocle2. **A** The cell trajectory state plot depicted the pseudo-temporal developmental trajectory of chondrocytes, wherein seven distinct cell states were visually distinguished and all cell subpopulations were represented along the trajectory. **B** The pseudotime plots depicted the sequential differentiation of chondrocytes. **C** Various subtypes of chondrocytes exhibited distinct differentiation trajectories within the cell type plot. **D** The heat map clearly revealed the distinct expression patterns of DEGs specific to branch point 1. **E** The utilization of pseudotime analysis resulted in the production of a heat map that visually represented the alterations in gene expression pertaining to the top 100 genes associated with cellular fate throughout the pseudotime continuum

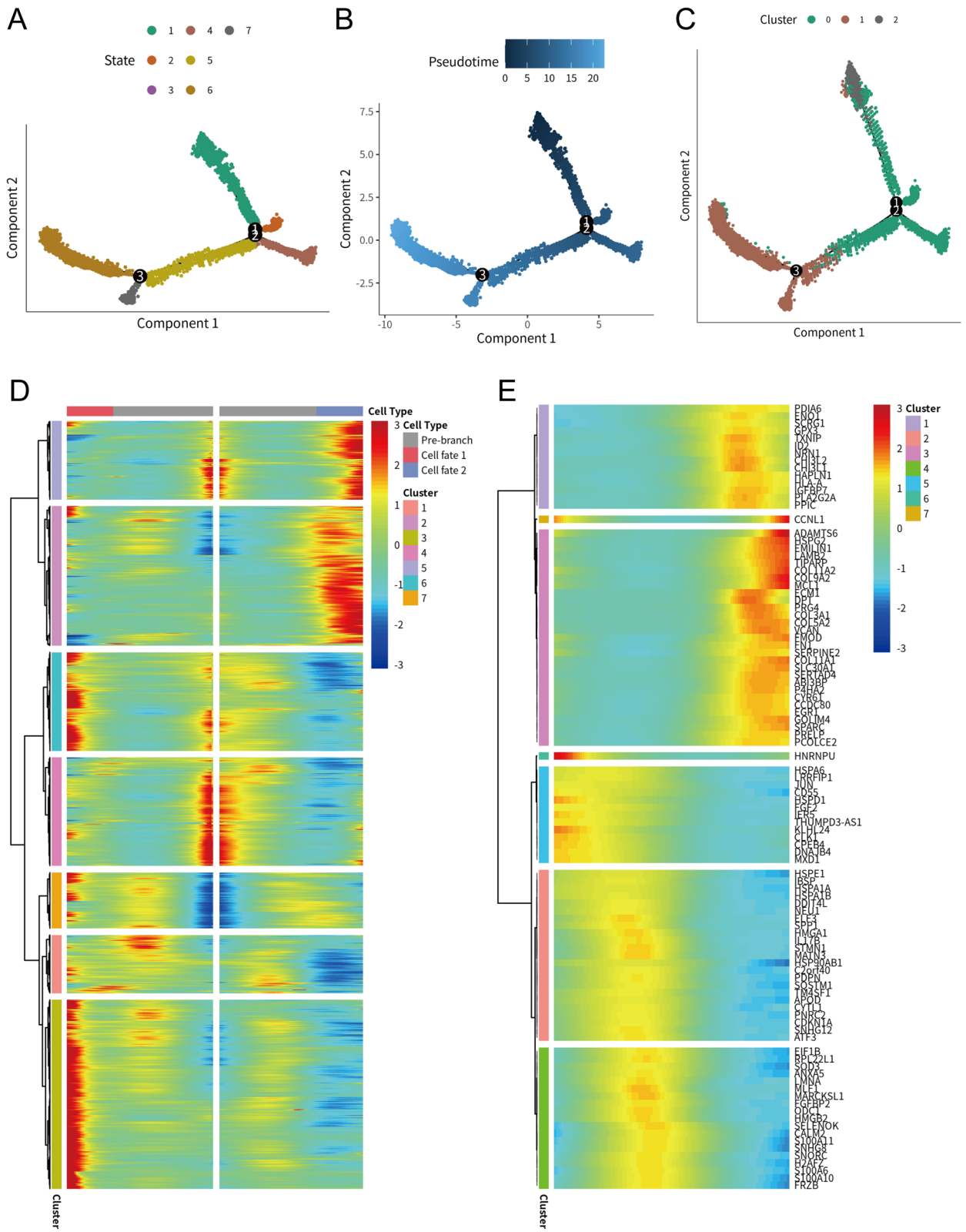

Fig. 3 (See legend on previous page.)

Construction of CDBIVDDC

To investigate the co-expression association among CDPRGs implicated in various stages of chondrocyte differentiation, we established a co-expression regulatory network determined through non-parametric tests and Pearson correlation (Fig. 4A). The genes responsible for directing chondrocyte differentiation were visually represented using distinct colors, while the positive and negative correlations between these genes were depicted through curves with paired symbols. Notably, the significant connectivity and associations among these crucial chondrocyte differentiation genes also elucidated the regulatory mechanisms underlying both clinical relevance and the fate of chondrocytes, as determined by this distinctive gene set.

According to Fig. 4A, a significant co-expression of all genes ($P<0.001$) was observed during the process of chondrocyte differentiation. Among these genes, 22 brown-labeled genes were identified as facilitators of the transition from chondrocytes to cellular state 2. These genes including *col1a2, lum, smoc2, htra1, aebp1* and more, which may participate in synthesis and remodeling of ECM. Additionally, 8 Gy-labeled genes (*tmsb10, sh3bgrl3, ifitm2, lgals1, s100a4, ssr4, ppib, ifitm1*), 6 purple-labeled genes (*mia, agr2, tuba1c, pthlh, pdlim4, ifit2*), and 3 yellow-labeled genes (*col6a2, antxr1, lyve1*) were found to be responsible for the transition to cellular state 7, cellular state 3, and cellular state 5, respectively. Furthermore, only one green-labeled gene (*f13a1*) and one yellow-green-labeled gene (*hspb1*) were found to be involved in the differentiation towards cell states 1 and 4, respectively. Furthermore, we conducted a functional enrichment analysis on the above genes, and the results showed that these genes could participate in VEGFA/VEGFR2 signaling, ECM organization, Interferon alpha/beta signaling, which are closely related to the occurrence and development of IVDD [69, 70] (Figure S4C).

Utilizing the aforementioned CDPRGs, the ConsensusClusterPlus algorithm was employed to conduct a consistency clustering analysis, resulting in the construction of a CDBIVDDC. Subsequently, model diagnosis was carried out. Notably, when the value of k was set to 3, the internal heterogeneity of the model exhibited enhanced discrimination (Fig. 4B, C). Consequently, the CDBIVDDC was partitioned into three distinct subtypes, namely Cluster 1, Cluster 2, and Cluster 3. The expression levels of CDPRGs within these subtypes, along with the chondrocyte differentiation status and varying degeneration levels, were visually represented through a heat map (Fig. 4D). It was worth mentioning that CDPRGs exhibited a predominant expression in Cluster 2, while displaying relatively lower expression levels in Clusters 1 and 3.

Moreover, we have substantiated the significance of the correlation between CDBIVDDC and the extent of degeneration and Thompson grade through a chi-square test ($P<0.001$). Additionally, the distribution of MD and LD composition ratios, as well as Thompson grade, exhibited variations across the three clusters (Fig. 4E, F). Specifically, it was observed that Cluster 2 exhibited a higher prevalence of MD, accounting for 69% of this cluster. Conversely, Cluster 1 and Cluster 3 had lower proportions of MD, with only 6% and 11% respectively. Additionally, Cluster 2 contained a higher percentage of Grade 5 (15%), Grade 4 (54%), and Grade 3 (31%) patients. On the other hand, LD was found to be more prevalent in Cluster 1, accounting for 94% of this cluster. In Cluster 2 and Cluster 3, LD accounted for 31% and 89% respectively. Furthermore, Cluster 1 contained a higher proportion of Grade 4 (6%), Grade 3 (50%), Grade 2 (38%), and Grade 1 (6%) patients. Overall, it could be concluded that Cluster 2 had the poorest prognosis in patients with IVDD, while Cluster 1 exhibited the most favorable prognosis and Cluster 3 had a moderate clinical prognosis.

PCA and IVDD clinical relevance analysis

In order to gain a deeper understanding of the molecular pathological attributes of chondrocytes within three clusters of CDBIVDDC, PCA was conducted on each

(See figure on next page.)

Fig. 4 Clustering consensus and clinical correlation. **A** An overview of the regulatory network associated with crucial genes involved in chondrocyte differentiation. The genes were depicted as circles, with their colors indicating the corresponding chondrocyte fates. The lines connecting the circles represented statistically significant correlations, denoted by a *P* value of less than 0.0001. Pink lines indicated positive correlations, while blue lines indicated negative correlations. Additionally, a nonparametric test revealed an inverse association between the size of the circles and the corresponding *P* values. **B** The analysis of Consensus Clustering successfully identified three distinct clusters within the IVDD microarray data obtained from GEO, utilizing key genes associated with chondrocyte differentiation. **C** The delta plots depicted alterations in the area under the cumulative distribution function (CDF) curve with respect to varying values of *k*. **D** An illustration of the cluster heat map generated through consensus clustering for the set of genes associated with chondrocyte differentiation. **E** The results of Pearson's chi-squared test indicated a statistically significant variation in the proportions of different degrees of degeneration across the three consensus clusters ($P<0.001$). **F** The findings from Pearson's chi-squared test revealed a statistically significant discrepancy in the proportions of various Thompson grading categories among the three consensus clusters ($P<0.001$)

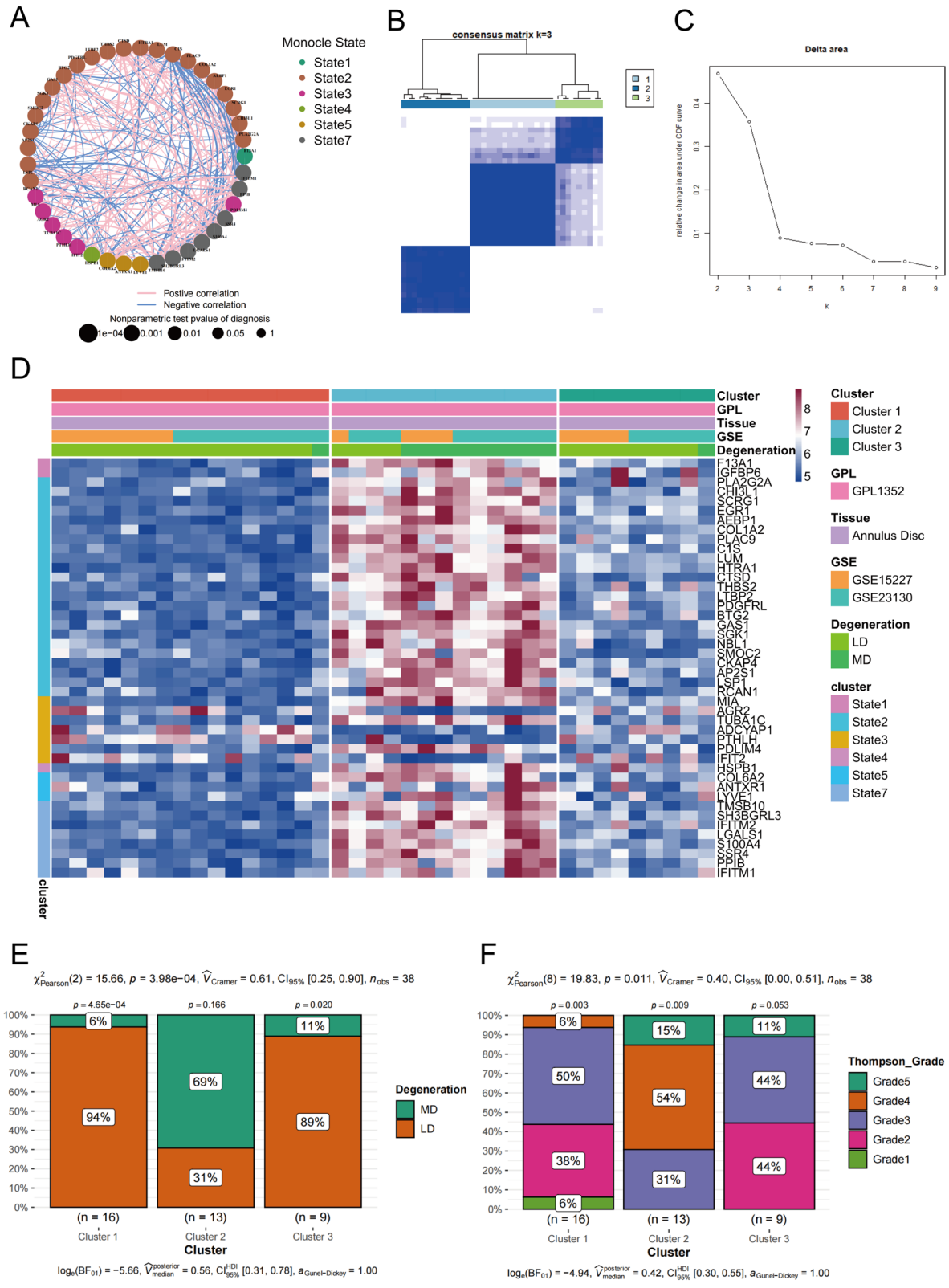

Fig. 4 (See legend on previous page.)

subtype. Subsequently, the chondrocyte score was computed for each cluster, and the scatter plot visually represented the variation in chondrocyte score across the different clusters (Figure S7A). Additionally, the box plot demonstrated statistically significant disparities in chondrocyte score among the three clusters ($P < 0.001$) (Figure S7B). Simultaneously, the chondrocyte score was partitioned into a high score group and a low score group, utilizing the median as the dividing point. This division aimed to investigate the potential association between the chondrocyte score and the extent of degeneration, as well as the Thompson grade, among patients with IVDD.

The presented bar graph illustrated the distribution of degeneration degrees in the high- and low-grade chondrocyte score groups, revealing that the low-grade chondrocyte score group consisted of 58% MD and 42% LD, while the high-grade chondrocyte score group exclusively comprised LD (Figure S7C). Furthermore, the accompanying block diagram displayed the varying proportions of MD and LD in the high and low scoring chondrocyte score groups ($P < 0.001$), thereby indicating a significant decline in chondrocyte score as degeneration increases ($P < 0.001$) (Figure S7D). Furthermore, the bar chart revealed a higher prevalence of samples with elevated Thompson grade in the low PCA chondrocyte score group (16% of grade 5; 42% of grade 4; 37% of grade 3; 5% of grade 2), while samples with lower Thompson grade were more prevalent in the high PCA chondrocyte score group (47% of grade 3; 47% of grade 2; 5% of grade 1) (Figure S7E). This observation suggested a progressive decrease in PCA chondrocyte score with an increase in Thompson grade. Correlations between PCA chondrocyte score and each Thompson grade displayed by the box plot (Figure S7F).

Among the three clusters of CDBIVDDC, it was observed that Cluster 1 exhibited the highest chondrocyte score, Cluster 2 had the lowest chondrocyte score, and Cluster 3 had a median chondrocyte score. Consequently, the three clusters of CDBIVDDC were designated as follows based on their respective chondrocyte score values: Cluster 1 was identified as the High Chondrocyte Scoring Classification (HCSC), Cluster 2 as the Low Chondrocyte Scoring Classification (LCSC), and Cluster 3 as the Medium Chondrocyte Scoring Classification (MCSC).

Meanwhile, Figure S7G demonstrated a statistically significant disparity in the relative expression levels of CDPRGs among the three clusters ($P < 0.001$). It was noteworthy that LCSC exhibited higher expression levels of most CDPRGs compared to the other clusters, which aligned with the aforementioned findings. Furthermore, the selection of key marker genes for each cluster was based on the relatively elevated expression of CDPRGs within the respective cluster: HCSC (Cluster 1) displayed relatively high expression of *adcyap1* and *pthlh*, LCSC (Cluster 2) exhibited relatively high expression of *mia* and *tuba1c*, and MCSC (Cluster 3) demonstrated relatively high expression of *lgals1* and *agr2*.

Descriptive statistics of baseline information in follow-up study of patients with IVDD

Between March 1, 2022 and June 1, 2023, a cohort of 98 patients diagnosed with IVDD were enrolled in the study, all of whom underwent decompression and fusion surgery for intervertebral discs. Among them, 38 patients were excluded from the study due to irregular completion of the ODI scale in 18 patients, a history of spinal fracture resulting from prior trauma in 10 patients, a history of spinal cord injury in 8 patients, and a combined diagnosis of spinal tumor or spinal metastasis in 2 patients. Ultimately, the study population consisted of 60 eligible patients, as illustrated by the flow chart that was compiled (Figure S8A).

Table S5 presented a comprehensive overview of the clinical baseline characteristics of 60 patients diagnosed with IVDD who satisfied the inclusion criteria for this study. Among these patients, 26 individuals (43.33%) were male, with an average age of 51.92 ± 15.16 years, while 34 individuals (56.67%) were female, with an average age of 56.35 ± 14.90 years. The age distribution was further categorized into three groups: 20 to 40, 41 to 60, and 61 to 90, and subsequently transformed into unordered categorical variables. The distribution of Pfirrmann grades among the 60 patients was as follows: Grade 3 in 11 individuals (18.33%), Grade 4 in 37 individuals (61.67%), and Grade 5 in 12 individuals (20%). Furthermore, the ODI scale scores of the patients were categorized into two groups based on a threshold of 50 points: the ODI low-score group (≤ 50 points) and the ODI high-score group (> 50 points). These groups accounted for 28 (46.67%) and 32 (53.33%) of the patients, respectively, thus forming a binary variable for further analysis in the study. Additionally, a heat map was employed to visually present the baseline information of patients diagnosed with IVDD (Figure S8B).

IHC of clinical samples in patients with IVDD

In order to investigate the clinical translational capacity of molecular typing, we conducted IHC staining on the acquired clinical specimens. Figure 5A presented the IHC staining outcomes of intervertebral disc samples extracted from patients diagnosed with IVDD through surgical intervention. The staining intensity of six marker proteins (ADCYAP1, PTHLH, MIA, TUBA1C, LGALS1, and AGR2) associated with CDBIVDDC, along with the proportion of positively stained cells within the

sections, were comprehensively evaluated by pathological experts. Based on the aforementioned scores, we categorized the samples into three distinct subgroups. The first subgroup, denoted as HCSC, exhibited a relatively high expression of PTHLH and ADCYAP1, while displaying a moderate or low expression of MIA, TUBA1C, LGALS1, and AGR2. The second subgroup, referred to as LCSC, demonstrated a relatively high expression of MIA and TUBA1C, alongside a medium or low expression of ADCYAP1, PTHLH, LGALS1, and AGR2. Lastly, the third subgroup, designated as MCSC, displayed a relatively high expression of LGALS1 and AGR2, accompanied by a moderate expression of MIA, TUBA1C, ADCYAP1, and PTHLH. According to the IHC staining results, it was observed that among the 60 patients analyzed, they were categorized into distinct molecular subtypes. Specifically, the HCSC group comprised 14 individuals (23.33%), the LCSC group consisted of 30 individuals (50%), and the MCSC group included 16 individuals (26.67%) (Table S5).

Single factor analysis of clinical baseline information for IVDD

The clinical baseline information of patients with IVDD was utilized as the independent variable, while the outcome variable was determined by whether the ODI scale score exceeded 50. A chi-square test was conducted to analyze the data. The results depicted in the Fig. 5B indicated that age, gender, occupation, smoking history, Pfirrmann classification, whether patients visited and underwent surgical treatment for Adjacent segment degeneration (ASD), and the molecular typing group of IVDD patients were all significantly associated with the ODI scale score. Specifically, in the high ODI group, the proportion of women was found to be higher than that of men ($P<0.05$), and the proportion of patients with Pfirrmann Grade 5 was also higher ($P<0.05$). It was worth mentioning that within the context of CDBIVDDC, the LCSC group demonstrated the highest proportion among individuals classified in the ODI high group (***$P<0.001$), thereby indicating that LCSC may be considered a risk factor for elevated ODI scores. Furthermore, the Pearson chi-square test and the Welch t test were conducted to analyze the data. As depicted in the Fig. 5C, a notable disparity was observed in the composition ratio of the three clusters of CDBIVDDC between the high scores and low scores groups on the ODI scale ($P<0.001$). Specifically, the proportion of LCSC in the high scores group was higher compared to the low scores group, whereas the proportion of HCSC in the high scores group was lower than that in the low scores group. The comparison of high-group scores in the ODI revealed a significantly higher proportion of LCSC (75%) compared to MCSC (16%) and HCSC (9%) ($P<0.001$). Moreover, the scatter plot and violin plot of the graph displayed the distribution and median ODI scale scores among patients in the three clusters of CDBIVDDC, followed by the Welch t test. The results indicated that the median ODI scores differ significantly among patients in the three clusters of IVDD ($P<0.001$), with LCSC patients exhibiting higher median ODI scores compared to those in the MCSC and HCSC groups $P<0.001$) (Fig. 5D). Simultaneously, the Pfirrmann grade was employed as the dependent variable, while CDBIVDDC was utilized as the independent variable for the chi-square test. The findings demonstrated a significant disparity in the composition ratio of the three clusters of CDBIVDDC across different Pfirrmann grades ($P<0.001$). Specifically, the proportion of the LCSC group was greater in Grade 5 compared to Grades 3 and 4, whereas the proportion of the HCSC group was higher in Grade 3 compared to Grades 4 and 5. Furthermore, Grade 5 exhibited the highest proportion of LCSC ($P<0.001$), accounting for 92% of the cases (Fig. 5E).

(See figure on next page.)

Fig. 5 IHC staining and single factor analysis of clinical samples from IVDD patients. **A** IHC staining of clinical samples. The IHC results were evaluated by pathologists who assigned scores based on the intensity of staining and the proportion of positive cells. A sample was categorized as HCSC if the expression of PTHLH and ADCYAP1 was high, while the expression of MIA, TUBA1C, LGALS1, and AGR2 was medium or low. Conversely, a sample was classified as LCSC if the expression of MIA and TUBA1C was relatively high, and the expression of ADCYAP1, PTHLH, LGALS1, and AGR2 was medium or low. Lastly, a sample was considered as MCSC if the expression of LGALS1 and AGR2 was high, and the expression of MIA, TUBA1C, ADCYAP1, and PTHLH was moderate. **B** The independent variable in this study was the clinical baseline information of patients with IVDD, while the outcome variable was determined based on whether the ODI scale score exceeded 50. To analyze the data, a chi-square test was performed. **C** The data was analyzed using the Pearson chi-square test and the Welch t test. A significant discrepancy was observed in the composition ratio of the three clusters of CDBIVDDC between the groups with high scores and low scores on the ODI scale ($P<0.001$). **D** The scatter plot and violin plot were utilized to visually represent the distribution and median ODI scale scores among patients categorized into three clusters of CDBIVDDC. Subsequently, the Welch t test was conducted to analyze the data. The findings revealed a significant difference in median ODI scores among patients in the three IVDD clusters ($P<0.001$). Specifically, LCSC patients exhibited notably higher median ODI scores compared to both the MCSC and HCSC groups ($P<0.001$). **E** The Pfirrmann grade was utilized as the dependent variable, whereas CDBIVDDC was employed as the independent variable for the chi-square test. The results revealed a significant discrepancy in the composition ratio of the three clusters of CDBIVDDC across various Pfirrmann grades ($P<0.001$)

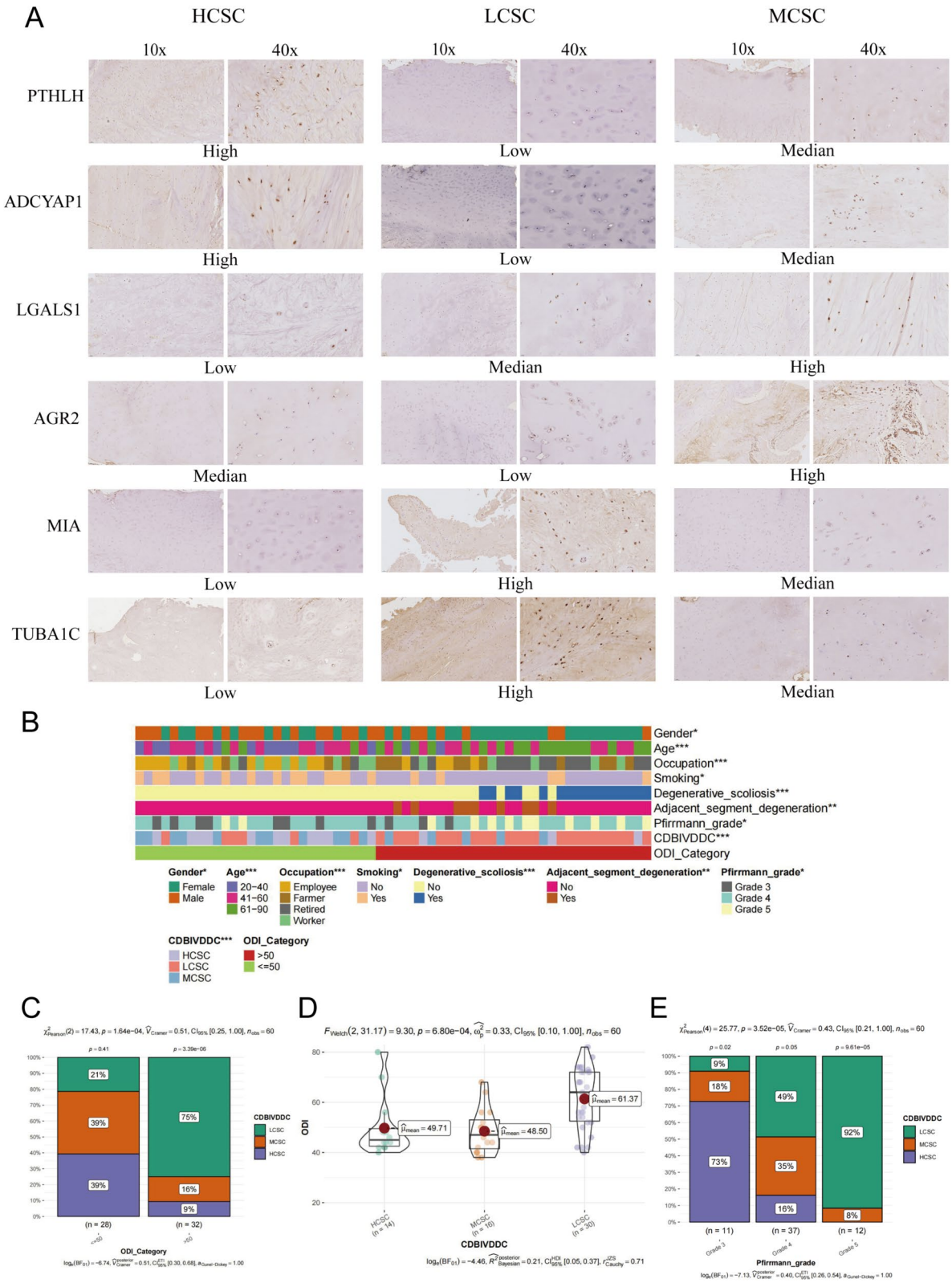

Fig. 5 (See legend on previous page.)

In conclusion, our findings indicated that patients with IVDD classified as LCSC exhibited higher ODI scores and Pfirrmann grades, which were indicative of more severe clinical symptoms, diminished quality of life, and unfavorable disease prognosis and outcome. This suggested that LCSC serves as a risk factor for poor prognosis and outcome. Conversely, patients with IVDD included in HCSC displayed lower ODI scores and Pfirrmann ratings, indicating milder clinical symptoms and more favorable prognosis and outcome. Consequently, our study highlighted the potential clinical translational significance of CDBIVDDC.

Prediction and in vitro experiments of small molecule targeted drugs for CDBIVDDC

In order to explore potential therapeutic approaches for IVDD, the gene expression matrix of the three clusters was utilized to assess the response sensitivity of each cluster to different small molecule targeted drugs. This analysis was performed using the pRRophetic package in the R programming language, as depicted in the violin plot (Fig. 6A). The specific targeted drugs examined were AZD.0530-HCSC, Gefitinib-LCSC, and CGP.082996-MCSC. One of the selected drugs for subsequent in vitro study was gefitinib, which specifically targeted the clinical poor prognosis cluster known as LCSC.

In order to further explore the impact of gefitinib on degenerated chondrocytes, we divided the chondrocytes into three groups. Ctrl, IL-1β, and IL-1β + Gefitinib group. Ctrl group mean cells cultured under normal conditions. Cells were stimulated with 10 ng/ml IL-1β for 24 h in IL-1β group. In IL-1β + Gefitinib group, cells were stimulated with 10 ng/ml IL-1β for 24 h, and then intervened with10μM gefitinib for 48 h.

The result of CCK-8 assay were presented in Fig. 6B. In comparison to the Ctrl group, IL-1β group exhibited a notable reduction in proliferation activity, while IL-1β + Gefitinib group demonstrated the ability to enhance proliferation capacity compared with IL-1β group (Fig. 6C). Toluidine blue staining was employed to examine the chondrocyte morphology. Chondrocytes in the Ctrl group exhibited a short and polygonal shape, with distinct staining of the ECM and a well-defined nucleus. Conversely, in the degeneration group (IL-1β group), there was a notable transformation in cell morphology, characterized by significant elongation and a spindle-shaped appearance. Additionally, the intensity of ECM staining was relatively diminished, and the nuclear boundary appeared indistinct. Furthermore, the IL-1β + Gefitinib group exhibited a substantial restoration in morphology compared to IL-1β group; the cells displayed a polygonal shape, and the intensity of ECM staining was notably profound (Fig. 6D), which is closely resembling that of the Ctrl group.

Furthermore, we examined the impact of gefitinib on the mRNA and protein expression of genes associated with chondrocyte synthesis and catabolism, as well as molecular typing markers (Fig. 6E, F). Compared to Ctrl group, the expression of COL2 and SOX9 were decreased and the expression of MMP13 was notably increased in chondrocytes of IL-1β group, indicating the the impaired function of chondrocytes. Following treatment with gefitinib (IL-1β + Gefitinib group), the mRNA and protein levels of COL2 and SOX9 in chondrocytes exhibited an increase, while MMP13 displayed a decrease compared to IL-1β group. These findings suggested that gefitinib has the potential to enhance the synthesis capability of chondrocytes. In relation to the molecular subtyping of IVDD,

(See figure on next page.)

Fig. 6 Prediction and in vitro experiments on small molecule targeted drugs for the treatment of CDBIVDDC. **A** The violin plot analysis revealed that the specific targeted drugs under investigation were AZD.0530-HCSC, Gefitinib-LCSC, and CGP.082996-MCSC. Among these drugs, Gefitinib was chosen for further in vitro experimentation due to its specific targeting of the LCSC cluster, which is associated with a clinically unfavorable prognosis. **B** The OD values of chondrocytes were compared between groups at each time point. **C** The graph exhibited a notable decline in proliferative activity within the degenerative model group (IL-1β group) in comparison to the control group (Ctrl). Nevertheless, the administration of gefitinib treatment (IL-1β + Gefitinib group) demonstrated the potential to augment proliferative capacity, as evidenced by a statistically significant disparity. **D** The findings from toluidine blue staining revealed distinct differences in chondrocyte morphology between the control group and the degenerative group. Chondrocytes in the control group exhibited a short and polygonal shape, with evident ECM staining and well-defined nuclei. Conversely, chondrocytes in the degenerative group displayed elongated and spindle-shaped morphology, accompanied by light ECM staining and indistinct nuclear boundaries. Notably, the administration of gefitinib resulted in a significant restoration of chondrocyte morphology, resembling that of the control group. The cells exhibited a polygonal morphology, while the intensity of ECM staining was notably profound. **E** The mRNA expression levels of genes associated with chondrocyte synthesis, catabolism, and IVDD molecular typing were assessed using qRT-PCR. (The sample size was n = 3. Statistical comparisons were made with a control group, denoted by $^{*}P < 0.05$, $^{**}P < 0.01$, and $^{***}P < 0.001$. Additionally, comparisons were made with the degeneration group, with statistical significance indicated by #, ##, ###, and #### for *P* values less than 0.05, 0.01, 0.001, and 0.0001, respectively). **F** A Western Blot analysis was conducted to ascertain the expression of genes associated with chondrocyte synthesis, catabolism, and IVDD molecular typing within each group. (The sample size was n = 3. Statistical comparisons were made against the control group, denoted by $^{*}P < 0.05$, $^{**}P < 0.01$, and $^{***}P < 0.001$. Additionally, comparisons were made against the degeneration group, indicated by $^{\#}P < 0.05$, $^{\#\#}P < 0.01$, and $^{\#\#\#}P < 0.001$)

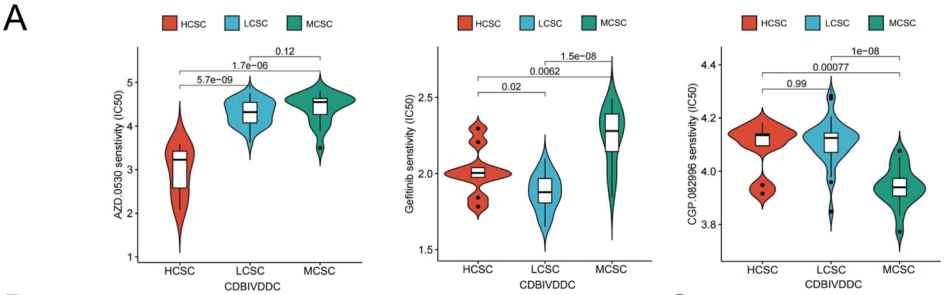

B

Experimental group	Ctrl	IL-1β	IL-1β+Gefitinib
0h OD value	0.630	0.608	0.622
	0.605	0.616	0.618
	0.615	0.623	0.615
24h OD value	1.156	0.801	0.810
	1.149	0.772	0.865
	1.135	0.809	0.836
48h OD value	2.022	1.373	1.643
	2.060	1.353	1.711
	2.042	1.327	1.694

OD: Optical Density

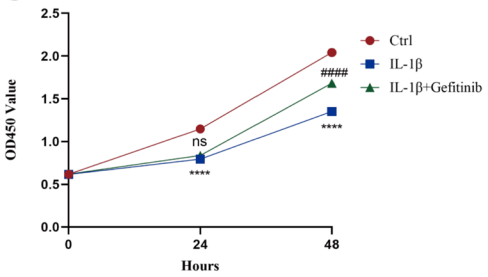

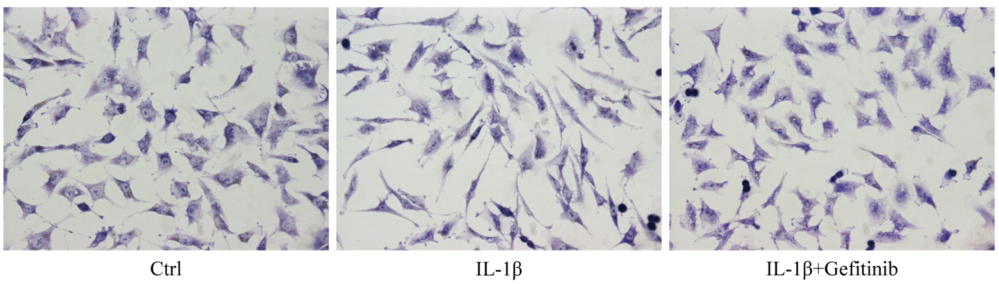

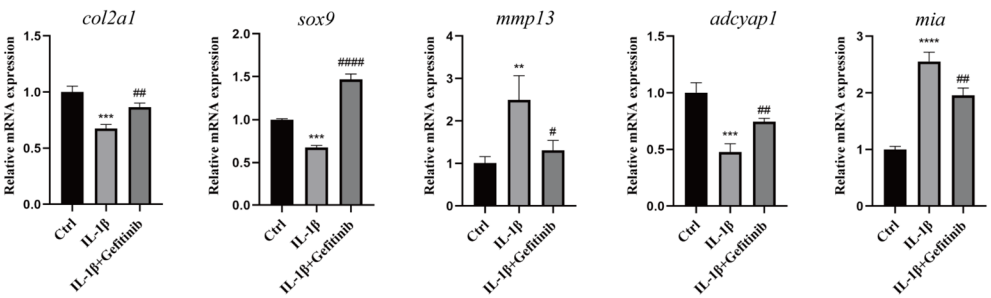

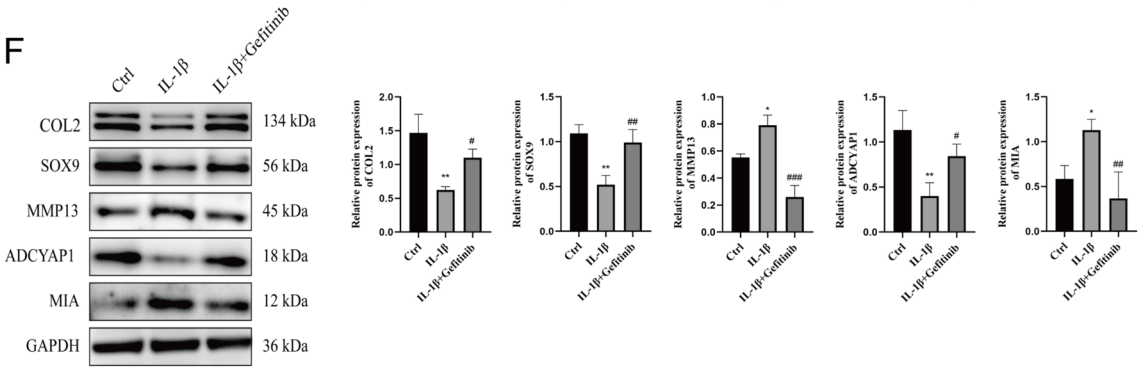

Fig. 6 (See legend on previous page.)

there was a decrease in the expression of ADCYAP1, a marker gene associated with the most favorable prognosis subtype, in the degeneration group (IL-1β group) compared to the Ctrl group; the expression of MIA, a marker gene associated with the least favorable prognosis subtype, was increased. However, gefitinib intervention (IL-1β + Gefitinib group) could reverse the change of ADCYAP1 and MIA expression in IL-1β group, indicating the potential of gefitinib to facilitate the conversion of chondrocytes into a more favorable prognosis type.

Discussion

Establishment of IVDD molecular typing

Despite some notable advancements in basic research and targeted interventions for the cause of IVDD, the intervertebral disc is a cart there remains a dearth of effective means and tools to implement precise interventions and impede the progression of IVDD. The advent of scRNA-seq and multiomics in the early twenty-first century has brought about transformative changes in the entire medical industry, encompassing basic research as well as disease diagnosis and treatment [71–73]. Leveraging this technological breakthrough, numerous scholars had sequentially delved into the progress of IVDD, aiming to unravel the intricate network mechanism underlying complex pathophysiology [74, 75].

Extensive research has demonstrated the pivotal involvement of chondrocytes in the pathogenesis of IVDD, thus establishing them as the primary instigators of this condition [76]. In this study, we conducted an analysis on two AF samples using a publicly available database. We obtained a total of 27,001 cells after scRNA-seq QC. Subsequently, we reduced the dataset and identified six distinct cell types, namely blood cells, chondrocytes, endothelial cells, NPPC, pericyte, and stromal cells. Notably, chondrocytes constituted the majority of the sample, accounting for 25,974 cells. We then focused on these chondrocytes for pseudo-timing analysis, which revealed seven different cell differentiation states and the identification of 1,058 CDGs. Furthermore, utilizing the IVDD microarray data, genes associated with the degenerative severity of IVDD patients were identified and extracted. These genes were then intersected with the aforementioned CDGs, resulting in the acquisition of 44 CDPRGs. Subsequently, the CDBIVDDC was constructed using ConsensusClusterPlus Consistent Clustering, employing the CDPRGs. Upon categorizing IVDD into three clusters, it was observed that CDPRGs exhibited a generally elevated expression level in Cluster 2. Subsequent studies have provided additional evidence supporting a significant correlation between CDBIVDDC and the extent of degeneration and Thompson grade among patients with IVDD. Specifically, Cluster 2 exhibited a more severe degree of degeneration and a higher Thompson grade, whereas Cluster 1 patients displayed LD and a lower Thompson grade. Cluster 3 tended to fall between these two clusters. Notably, a lower chondrocyte score was indicative of more pronounced degeneration and a higher Thompson rating, while a higher chondrocyte score suggested the opposite relationship.

The three clusters in CDBIVDDC were designated and their corresponding marker genes were suggested based on the high and low chondrocyte scores, as well as the relatively elevated expression of CDPRGs. Cluster 1, referred to as HCSC, exhibited the most favorable prognosis and was characterized by the marker genes *adcyap1* and *pthlh*. Cluster 2, known as LCSC, displayed the poorest prognosis and was distinguished by the marker genes *mia* and *tuba1c*. Cluster 3, denoted as MCSC, demonstrated a moderate prognosis and was identified by the marker gene *lgals1* and *agr2*.

HCSC demonstrated the most favorable prognosis, with high expression of *adcyap1* and *pthlh*. *Adcyap1* is responsible for encoding the Pituitary Adenylate Cyclase Activating Polypeptide (PACAP), a neuropeptide that exhibited diverse functions such as neurotrophic, neuromodulatory, and neurotransmitter activities [77]. Additionally, ADCYAP1/PACAP served as an effective neuro and cell-protecting peptide, exerting anti-inflammatory, anti-apoptotic, and antioxidant effects [78–82]. Simultaneously, ADCYAP1/PACAP has been recognized as a proficient anti-inflammatory agent that operated through the regulation of anti-inflammatory and pro-inflammatory mediators [83–86]. Research had indicated that diminished levels of ADCYAP1/PACAP in the synovial fluid of joints may serve as an indicator of the extent of articular osteoarthritis (OA) subsequent to anterior cruciate ligament injury [87]. Furthermore, ADCYAP1/PACAP facilitated the regeneration of cartilage in the presence of articular inflammation or degeneration of articular cartilage [84]. Notably, age is widely recognized as a contributing factor to IVDD, and mice lacking ADCYAP1/PACAP demonstrated accelerated aging, indicating a potential protective role of ADCYAP1/PACAP in age-related degenerative processes [88]. Additionally, an increasing body of research has demonstrated the efficacy of ADCYAP1/PACAP in ameliorating cartilage degradation through diverse mechanisms [89].

The *pthlh* gene is situated on the p-arm of chromosome 12 and comprises three promoters and nine exons [90]. *Pthlh* played a crucial role in the regulation of cartilage formation, exerting its influence by promoting chondrocyte proliferation, impeding terminal differentiation, and delaying chondrocyte degeneration [91, 92]. Furthermore, *pthlh* suppressed the expression of *mmp13* in antler chondrocytes [93], whereas other investigations

have reported a significant elevation in the expression levels of type II collagen and proteoglycan due to *pthlh* [92]. In vivo experiments have demonstrated that the upregulation of the *pthlh* gene was associated with a reduction in chondrocyte apoptosis and chondrogenesis [93], whereas the knockout of the *pthlh* gene resulted in abnormal chondrodevelopment, expedited chondrocyte differentiation, and accelerated chondrocyte ossification [94, 95]. Furthermore, *pthlh* has been observed to impede chondrocyte hypertrophy and bone formation in vivo by inhibiting the Mef2/Runx2 signal cascade through the involvement of histone deacetylase 4 and histone deacetylase 5 [96, 97]. Collectively, the involvement of *adcyap1* and *pthlh* was crucial in preserving the chondrocyte phenotype and impeding degradation, thereby potentially serving as the most influential factors in determining the clinical prognosis of the HCSC subtype.

The worst prognostic LCSC cluster exhibited high expression levels of *mia* and *tuba1c*. *Mia*, alternatively referred to as Cartilage Derived Retinoic Acid Sensitive Protein (CD-RAP), is a small-secreted protein with a molecular weight of 11–14 kD [98]. It belongs to the extracellular protein family characterized by the Src Homology 3 (SH3) domain-like fold [99]. In normal physiological circumstances, *mia* was expressed in both embryonic and adult cartilage [100–102]. In addition, *mia* has been recognized as a marker indicative of the differentiation of chondrocytes and hold significant importance within the intricate regulatory system governing chondrocyte differentiation and stability [103–106]. In instances of pathological conditions, *mia* was observed to be present in diverse tumor tissues, including chondrosarcoma and melanoma [107, 108]. Notably, *mia* exhibited potential as a serum and synovial marker for the early stages of OA joint alterations and degenerative processes, such as rheumatoid arthritis (RA) and OA [103, 104]. Research has demonstrated that the concentration of serum *mia* in individuals with RA was comparable to that observed in the majority of melanoma patients. It was hypothesized that a significant portion of *mia* was actively released by chondrocytes during the progression of joint deterioration, while another portion was passively released as a result of chondrocyte necrosis or apoptosis. Consequently, *mia* may serve as a potential indicator of chondrocyte destruction [103]. Findings from various investigations have indicated that lower concentrations of *mia* promoted the chemokinesis of mesenchymal stem cells, whereas higher concentrations of *mia* impeded their chemokinesis [99]. Moreover, *mia* exhibited a significant role as an autoantigen in influencing the pathogenesis of arthritis [109].

Tuba1c, a constituent of the alpha-tubulin proteins comprising microtubules, is implicated in cellular mitosis [110, 111]. Prior investigations have indicated that upregulation of *tuba1c* expression exerted a substantial influence on the growth and advancement of neoplastic cells, playing a pivotal role in the proliferation and cell cycle of diverse tumors [112, 113]. Recent scholarly inquiry has unveiled the potential involvement of microtubule structure and function in the innate and adaptive immune response [114]. The expression of *tuba1c* was found to be positively correlated with the infiltration of various immune cells, including B cells, CD8 + T cells, CD4 + T cells, macrophages, dendritic cells, and neutrophils [115]. This high expression of *tuba1c* in the LCSC cluster has the potential to enhance the inflammatory response within the intervertebral disc immune microenvironment and expedite IVDD, ultimately impacting the prognosis of patients. Consequently, the elevated expression of both the LCSC cluster *mia* and *tuba1c* in CDBIVDDC may contribute to heightened cartilage destruction and inflammatory response in individuals with IVDD, leading to an unfavorable prognosis.

The prognosis of MCSC is deemed moderate due to the high expression of *lgals1* and *agr2*. LGALS1 is a 14 kDa beta-galactoside binding protein that exhibits affinity towards various ECM proteins [116, 117]. Previous research has demonstrated the significant involvement of *lgals1* in the regulation of cell growth, adhesion, migration, apoptosis, and tissue development [118]. Simultaneously, *lgals1* exhibited immunosuppressive and anti-inflammatory properties in numerous chronic inflammatory and autoimmune disorders [119, 120]. Research has demonstrated that both *lgals1* gene therapy and recombinant intra-articular administration of LGALS1 could mitigate arthritis manifestation in murine models [121]. Furthermore, *lgals1* was believed to play a pivotal role in cartilage regeneration [122]. However, previous research has demonstrated that the upregulation of *lgals1* was correlated with the severity of degeneration in osteoarthritic cartilage and subchondral tissue. Additionally, these findings highlighted *lgals1* as a significant regulator of inflammatory response genes that are clinically relevant [123]. Another protein, AGR2, which belongs to the protein disulfide isomerase family, has been found to play a crucial role in inhibiting the inflammatory response mediated by the NF-κB signaling pathway [124]. Consequently, it could be concluded that the high expression of *lgals1* and *agr2* may contribute to a more favorable prognosis in patients with MCSC cluster compared to those with LCSC cluster.

Validation of IVDD molecular typing in clinical case–control study

In the light of the aforementioned molecular typing of IVDD, we conducted a clinical case–control study

to investigate its potential translational medicine significance. IHC employs the principle of antigen–antibody binding to investigate the spatial distribution, qualitative characteristics, and quantitative aspects of antigens within tissues, accomplished through the observation of color development resulting from labeled antibody interactions [125]. This technique holds significant value in bridging the gap between molecular investigations and clinical applications, finding extensive utilization in both fundamental pathological diagnosis and clinical research endeavors [126–128]. In this study, disc tissue was extracted from patients who met specific inclusion and exclusion criteria, followed by IHC staining. The staining intensity and percentage of chondrocytes were subsequently evaluated and categorized. The staining results revealed a notable differentiation and discrimination among the six marker genes of the three clusters. Based on the relative expression levels of these marker genes, the samples were then classified into three groups (HCSC, LCSC, and MCSC groups), serving as one of the independent variables in the study.

Furthermore, the evaluation of clinical symptom severity, quality of life, and dysfunction of patients was conducted using ODI scale scores and Pfirrmann rating of MRI, which were chosen as outcome variables in this study. The findings of the study were found to align with our initial research hypotheses. Specifically, patients in the HCSC group exhibited a low ODI score, indicating mild clinical symptoms and a relatively high quality of life. Conversely, patients in the LCSC group demonstrated a high ODI score, indicating more severe clinical symptoms, a diminished quality of life, and noticeable dysfunction. At the imaging level, the study revealed variations in the extent of IVDD among the three subgroups. Specifically, the HCSC subgroup exhibited mild degeneration, while the LCSC subgroup displayed the most severe degeneration. The findings of this study implied that the three clusters of CDBIVDDC possessed distinctive and predictive capabilities, all of which could effectively reflect the severity of degeneration in patients with IVDD.

In short, our study has established that the three categories of CDBIVDDC have demonstrated effectiveness in differentiating the severity of the disease and accurately forecasting its prognosis in the clinical practical implementation among patients with IVDD. As a result, these categories could serve as a valuable instrument for healthcare professionals in categorizing patients' risks and expediting the decision-making procedures.

Prediction of drugs targeting small molecules and experimental study in vitro

The pRRophetic software, created by Paul Geeleher and colleagues at the University of Minnesota, emerged from their research conducted in 2014 [129, 130]. This software package primarily served the purpose of predicting phenotypic outcomes of gene expression microarray data. It accomplished this by utilizing sensitivity data from 138 drugs across over 700 cell lines available in the Cancer Genome Project (CGP) database, and employing statistical models to achieve accurate predictions [131]. Furthermore, empirical investigations have demonstrated that the pRRophetic package possessed the capability to not only forecast the specific drug responsiveness of primary tumor sample cell lines, but also to facilitate the construction of models for diverse cell lines and clinical datasets [132, 133].

Moreover, by employing the pRRophetic package, we made prognostic estimations regarding the distinct susceptibility levels of the three clusters of CDBIVDDC. It was noteworthy to mention that the compound anticipated by LCSC was gefitinib, an epidermal growth factor receptor (EGFR) inhibitor that has received approval from the Food and Drug Administration (FDA) [134]. Gefitinib functions by competitively binding to ATP, thereby impeding EGFR activity [134]. Moreover, a plethora of studies have extensively showcased the role of transforming growth factor-α (TGF-α) as a potent activator of the EGFR signaling pathway. The TGF-α/EGFR signaling axis has emerged as a crucial determinant in the modulation of cartilage synthesis and catabolic activity [135, 136], thereby exerting a substantial influence on the establishment of animal models for OA and the pathological mechanisms observed in OA patients [137–139]. A previous proteomic investigation conducted by Appleton et al. demonstrated the enrichment of proteins associated with EGFR signaling in individuals diagnosed with OA [140]. In a study conducted by Sun et al. in 2018, it was discovered that OA patients exhibited subpopulations with elevated levels of EGFR activation. Subsequent in vivo and in vitro experiments elucidated that this activation of EGFR was responsible for the imbalance of chondrocytes. Moreover, the study demonstrated that gefitinib effectively inhibited the stimulation of TGF-α, thereby inhibiting the EGFR signal axis. Additionally, the study proposed that localized controlled release of gefitinib within the joint enhanced the progression of the mouse OA model by suppressing the EGFR signal axis [135].

Moreover, Pan et al. conducted a study which provided evidence of a noteworthy presence of phosphorylated EGFR in damaged menisci of both mice and humans, indicating the activation and upregulation of the EGFR

signaling pathway in such instances. Furthermore, investigations involving *egfr* knockout mice demonstrated that a lack of *egfr* facilitated the production of supplementary extracellular matrices in these animals. Furthermore, in vitro experiments have shown that the administration of gefitinib effectively maintained fibrochondrocyte homeostasis and promotes meniscus regeneration in mouse models of meniscus injury through the inhibition of EGFR signaling pathways [141]. Another study conducted by Pan et al. investigated the expression of EGFR and the inhibition of autophagy in rat models of IVDD and IVDD patients. The study also examined the impact of *egfr* deficiency on ECM degradation in the intervertebral disc and the promotion of cellular autophagy in *egfr* knockout mice. Subsequent studies have further elucidated the role of gefitinib in maintaining nucleus pulposus cell phenotypes in rats through the EGFR/autophagy axis. Additionally, these studies have demonstrated that the controlled release of gefitinib in rat IVDD models may impede the process of IVDD via the EGFR/autophagy axis [142].

Additionally, a clinical case report has indicated that a 72-year-old female patient diagnosed with non-small cell lung cancer experienced a noteworthy amelioration in arthritis symptoms subsequent to the initial administration of gefitinib [143]. Moreover, a retrospective clinical study encompassing individuals diagnosed with non-small cell lung cancer and IVDD who were treated with gefitinib medications between 2010 and 2015, evaluated the extent of IVDD utilizing the Pfirrmann grading system. The findings indicate that patients treated with gefitinib exhibited a slower progression of IVDD. It was important to note that the study sample size did not reach statistical significance; however, these results suggested that gefitinib may hold promise as a potentially effective treatment for IVDD [142].

In this study, we investigated the impact of gefitinib on the in vitro model of chondrocyte degeneration induced by IL-1β, and examined the influence of gefitinib on the expression of molecular typing marker genes associated with IVDD. The results obtained from the CCK-8 assay indicated a significant decrease in cell proliferation activity in the IL-1β group. However, the IL-1β + Gefitinib group exhibited a reversal of this effect and demonstrated an improvement in cell proliferation ability. Furthermore, the application of toluidine blue staining revealed that the cellular morphology of the IL-1β group exhibited a spindle-shaped appearance, accompanied by a faint ECM staining and indistinct nuclear boundaries. Conversely, the IL-1β + Gefitinib group displayed a partial restoration of cellular morphology, characterized by a polygonal shape and intensified ECM staining. In addition, the results obtained from qPCR and Western Blot analyses revealed a significant decrease in the expression levels of COL2 and SOX9, accompanied by an increase in the expression levels of MMP13, within the IL-1β group. Conversely, following the intervention of gefitinib, there was a notable increase in the expression levels of COL2 and SOX9, coupled with a decrease in the expression levels of MMP13. These findings strongly indicated that gefitinib exhibited a remarkable ability to effectively retard the degeneration of chondrocytes induced by IL-1β, thereby enhancing their cellular functionality.

Moreover, gefitinib demonstrated a significant influence on the expression levels of molecular typing marker genes linked to IVDD. The analysis conducted using qPCR and Western Blot techniques unveiled an elevation in MIA expression level and a reduction in ADCYAP1 expression level in the IL-1β group compared to the Ctrl group. However, following intervention with gefitinib, the expression of MIA decreased while the expression of ADCYAP1 increased, with statistically significant differences observed. The results of this study indicated that gefitinib may have the potential to convert the LCSC cluster, which was linked to a poor prognosis in the molecular classification of IVDD, into the HCSC cluster, which was associated with a favorable prognosis. This study provided evidence supporting the potential clinical utility of gefitinib in the treatment of IVDD.

Limitation

Nevertheless, it was important to acknowledge the limitations of this study. Primarily, the reliance on pure bioinformatics analysis introduces a potential bias, limiting the comprehensive depiction of the chondrocyte development trajectory and the full spectrum of cell differentiation states in IVDD. Consequently, it was crucial to undertake further systematic basic experiments in the future to substantiate the clinical relevance of IVDD molecular typing from diverse viewpoints. Furthermore, the case–control study was carried out within the confines of a solitary hospital institution, resulting in a restricted sample size. Consequently, it was imperative to conduct subsequent large-scale, multi-center clinical studies to validate and reinforce these findings. Finally, despite being approved by the FDA, gefitinib encountered challenges in achieving clinical translation. Research has revealed that the administration of gefitinib on a large scale could expedite the advancement of OA and induce weight loss

[144], thereby imposing limitations on its clinical applicability due to the associated side effects.

Conclusion

In conclusion, our study presented a proposed molecular classification of IVDD through the integration of multi-omics information with single-cell technology. This classification not only encompassed the diverse molecular-level cell differentiation fate but also correlated with the varied prognostic outcomes observed in patients with IVDD in clinical settings. Furthermore, this classification demonstrated potential for molecular diagnosis and prediction of clinical prognosis. Subsequently, we validated the clinical applicability and transformative value of this proposed classification in IVDD patients through a case–control study. Our in vitro experimental investigation, based on this classification, demonstrated that gefitinib effectively delayed the degeneration of chondrocytes induced by IL-1β and exhibited the ability to convert the LCSC cluster to the HCSC cluster.

This study posited that CDBIVDDC possessed the ability to proficiently assess the severity of IVDD patients and precisely forecasted the prognosis and outcome of the disease. In practical application, CDBIVDDC could serve as a valuable instrument to aid clinicians in conducting risk assessment and clinical decision-making for IVDD patients, while also offering novel perspectives and concepts for the diagnosis and treatment of IVDD.

Abbreviations

DDD	Disc degenerative diseases
IVDD	Intervertebral disc degeneration
LBP	Lower back pain
CDGs	Chondrocyte differentiation-related genes
CDPRGs	Chondrocyte differentiation and prognosis related genes
PCA	Principal component analysis
AF	Annulus fibrosus
GEO	Gene Expression Omnibus
ScRNA-seq	Single cell RNA sequencing
RMA	Robust multi-array average
QC	Quality control
PCs	Principal components
UMAP	Uniform manifold approximation and projection for dimension reduction
DEG	Differential expression gene
FC	Fold change
FDR	False discovery rate
CDBIVDDC	Chondrocyte differentiation based IVDD classification
LD	Less degeneration
MD	More degeneration
IHC	Immunohistochemistry
ODI	Oswestry disability index
STROBE	Strengthening the Reporting of Observational Studies in Epidemiology
ADCYAP1	Adenylate cyclase activating polypeptide 1
PTHLH	Parathyroid hormone like hormone
MIA	Melanoma inhibitory activity
TUBA1C	Tubulin alpha 1c
LGALS1	Galectin-1
AGR2	Anterior gradient homologous protein-2
CCK-8	Cell Counting Kit-8
qPCR	Quantitative reverse transcription polymerase chain reaction
ECL	Enhanced chemiluminescence
COL2	Collagen type II
SOX9	SRY-box transcription factor 9
MMP13	Matrix metallopeptidase 13
HRP	Horseradish peroxidase
AF	Annulus fibrosus
NPPC	Nucleus pulposus progenitor cell
COL2A1	Collagen type II alpha 1 chain
CHAD	Chondroadherin
CD44	Cluster of differentiation 44
ECM	Extracellular matrix
MKI67	Marker of proliferation Ki-67
PDPN	Podoplanin
PNRC2	Proline-rich nuclear receptor co-activator 2
STMN1	Stathmin 1
ENO1	Alpha-enolase
PLA2G2A	Phospholipase A2, group IIA
HSPG2	Heparan sulfate proteoglycan 2
HV	Healthy volunteer
HCSC	High chondrocyte scoring classification
LCSC	Low chondrocyte scoring classification
MCSC	Medium chondrocyte scoring classification
ASD	Adjacent segment degeneration
OD	Optical density
Ctrl	Control group
PACAP	Pituitary adenylate cyclase activating polypeptide
OA	Osteoarthritis
CD-RAP	Cartilage derived retinoic acid sensitive protein
SH3	Src Homology 3
RA	Rheumatoid arthritis
CGP	Cancer genome project
EGFR	Epidermal growth factor receptor
FDA	Food and Drug Administration
TGF-α	Transforming growth factor-α

Supplementary Information

The online version contains supplementary material available at https://doi.org/10.1186/s12967-025-06225-8.

Additional file 1. The flow chart of the study (related to Fig. 1).

Additional file 2: Figure S2. Analyses integrated of differential expression genes, cellular communication, and cell cycle. **A** The Cleveland's dot plot depicted the expression levels of four classical marker genes; the stacked bar plot visually represented the proportion of six distinct cell types in two AF samples. **B** The heat map effectively visualized the expression levels of the top five marker genes in each cell type. **C** The iTalk network unveiled the intersecting cellular communication pathways among six distinct cells. **D** The ligand-receptor plot provided a comprehensive overview of the specific cell-to-cell communication mechanisms within the six distinct cell types. Additionally, it highlighted the key genes involved in facilitating this cellular communication. **E**. Functional enrichment analysis of genes with chondrocytes as ligands and receptors. **F** G2M. Score and S. Score of six distinct cell types were shown in the violin plots. **G** The feature plot showed the distribution of six distinct cell types at various stages of the cell cycle.

Additional file 3: Figure S3. Analysis of chondrocyte cell trajectory. **A** The cell type plot exhibited the specific chondrocyte subpopulation associated with each state. **B** The cell trajectory state plot depicted the presence of seven distinct cell states within chondrocyte clusters. Additionally, the plot revealed the occurrence of three branch pointsthat demarcated the divergence of differentiated fates. **C** The feature plot depicted the distribution of seven cell state clusters, as determined through dimension reduction analysis. **D** The presented pseudotime plot depicted the expression levels of pivotal marker genes across distinct stages of differentiation. **E** The pseudotime plot depicted the expression levels of pivotal marker genes within three chondrocyte clusters.

Additional file 4: Figure S4. Identification of key genes related to the fate of IVDD chondrocyte. **A** The Venn diagram depicted the presence of overlapping genes between the univariate regression analysis and pseudotemporal analysis, specifically referred to as CDPRGs. **B** The non-parametric tests revealed differential distribution of *adcyap1*, *pthlh*, *mia*, and *tuba1c* genes between Thompson I to III) and Thompson IV to V), as evidenced by the box plots. **C** The results of the functional enrichment analysis indicated that CDPRGs might take part in the VEGFA/VEGFR2 signaling pathway, ECM organization, and the Interferon alpha/beta signaling pathway, which were all intimately connected to the occurrence and advancement of IVDD.

Additional file 5: Figure S5. ScRNA-seq data external validation demonstrated the feature plots of CDPRGs. **A** UMAP dimensionality reduction analysis was performed on the intervertebral disc tissues of healthy volunteersand patients with IVDD, and five cell types were obtained. **B** The feature plots of CDPRGs demonstrated their distribution in cells and samples.

Additional file 6: Figure S6. ScRNA-seq data external validation demonstrated the expression level of CDPRGs in the intervertebral disc tissues of HV and IVDD.

Additional file 7: Figure S7. Correlation analysis of PCA chondrocyte score. **A** Based on the fundamental clustering of gene expression related to chondrocyte differentiation, the PCA scores demonstrated a tendency for samples within the same group to cluster together. **B** The Mann–Whitney U-test demonstrated statistically significant variations in the PCA chondrocyte scores among consensus clusters. **C** The bar plot depicted the percentage of samples exhibiting varying degrees of degeneration within the high and low PCA chondrocyte score groups. **D** The box plot demonstrated that the PCA chondrocyte score exhibited significant variation across various levels of degeneration. **E** The bar plot illustrated the distribution of samples with different Thompson grading percentages within the high and low PCA chondrocyte score groups. **F** The box plot revealed a statistically significant variation in PCA chondrocyte scores among samples with varying Thompson grading. **G** The expression of CDPRGs in different consensus clusters exhibit significant statistical differences.

Additional file 8: Figure S8. The inclusion and exclusion criteria and the comprehensive depiction of clinical baseline characteristics. **A** The flowchart visually depicted the procedure of study inclusion and exclusion. **B** The heat map was employed as a visual tool to effectively present baseline information pertaining to eligible patients with IVDD.

Additional file 9.

Additional file 10.

Additional file 11.

Additional file 12.

Additional file 13.

Acknowledgements
We thank the Gene Expression Omnibus (Accession no. GSE160756, GSE15227 and GSE23130) for using their data.

Author contributions
Shaofeng Chen and Yifan Liu collaborated in the process of co-authoring and revising the manuscript. Shaofeng Chen and Wei Zhang participated in the experiment. Runzhi Huang was accountable for formulating the overarching concept of the document and conducting bioinformatics analysis. Xianzhao Wei and Xiaoyi Zhou assumed responsibility for overseeing the conceptual framework of the manuscript and contributed to the collection of clinical samples.

Funding
This study was supported by the long-range navigation talent program in Navy Medical University.

Data availability
The original contributions presented in the study are included in the article. Further inquiries can be directed to the corresponding authors.

Declarations

Ethics approval and consent to participate
The Ethics Committee of Shanghai Changhai Hospital has granted approval for the protocol of this study, as indicated by the Ethics Approval Document No. CHEC2022-262.

Consent for publication
All authors have given their consent for publication.

Competing interests
The author declares no competing financial interests.

Author details
[1]Department of Orthopaedic Surgery, Changhai Hospital, Shanghai, China. [2]Department of Orthopaedic Surgery, China Coast Guard Hospital, Zhejiang, China. [3]Department of Burn Surgery, Changhai Hospital, Shanghai, China. [4]Research Unit of Key Techniques for Treatment of Burns and Combined Burns and Trauma Injury, Chinese Academy of Medical Sciences, Shanghai, China. [5]Department of Urology, Xinhua Hospital Affiliated to Shanghai Jiao Tong University School of Medicine, Shanghai, China. [6]BGI research, BGI-Hangzhou, 310012 Hangzhou, China.

Received: 11 March 2024 Accepted: 11 February 2025
Published online: 25 February 2025

References

1. Wu PH, Kim HS, Jang IT. Intervertebral disc diseases part 2: a review of the current diagnostic and treatment strategies for intervertebral disc disease. Int J Mol Sci. 2020;21(6):2135.
2. Urban JP, Roberts S. Degeneration of the intervertebral disc. Arthritis Res Ther. 2003;5(3):120–30.
3. Adams MA, Roughley PJ. What is intervertebral disc degeneration, and what causes it? Spine (Phila Pa 1976). 2006;31(18):2151–61.
4. Hadjipavlou AG, Tzermiadianos MN, Bogduk N, Zindrick MR. The pathophysiology of disc degeneration: a critical review. J Bone Joint Surg Br. 2008;90(10):1261–70.
5. Feng Y, Egan B, Wang J. Genetic factors in intervertebral disc degeneration. Genes Dis. 2016;3(3):178–85.
6. Vergroesen PP, Kingma I, Emanuel KS, Hoogendoorn RJ, Welting TJ, van Royen BJ, et al. Mechanics and biology in intervertebral disc degeneration: a vicious circle. Osteoarthritis Cartilage. 2015;23(7):1057–70.
7. Mayer JE, Iatridis JC, Chan D, Qureshi SA, Gottesman O, Hecht AC. Genetic polymorphisms associated with intervertebral disc degeneration. Spine J. 2013;13(3):299–317.
8. Stewart WF, Ricci JA, Chee E, Morganstein D, Lipton R. Lost productive time and cost due to common pain conditions in the US workforce. JAMA. 2003;290(18):2443–54.
9. Hoy D, March L, Brooks P, Blyth F, Woolf A, Bain C, et al. The global burden of low back pain: estimates from the Global Burden of Disease 2010 study. Ann Rheum Dis. 2014;73(6):968–74.
10. Livshits G, Popham M, Malkin I, Sambrook PN, Macgregor AJ, Spector T, et al. Lumbar disc degeneration and genetic factors are the main risk factors for low back pain in women: the UK Twin Spine Study. Ann Rheum Dis. 2011;70(10):1740–5.
11. Krut Z, Pelled G, Gazit D, Gazit Z. Stem cells and exosomes: new therapies for intervertebral disc degeneration. Cells. 2021;10(9):2241.
12. Wong JJ, Côté P, Sutton DA, Randhawa K, Yu H, Varatharajan S, et al. Clinical practice guidelines for the noninvasive management of low back pain: a systematic review by the Ontario Protocol for Traffic Injury Management (OPTIMa) Collaboration. Eur J Pain. 2017;21(2):201–16.
13. Sampara P, Banala RR, Vemuri SK, Av GR, Gpv S. Understanding the molecular biology of intervertebral disc degeneration and potential

gene therapy strategies for regeneration: a review. Gene Ther. 2018;25(2):67–82.
14. Sakai D, Schol J. Cell therapy for intervertebral disc repair: clinical perspective. J Orthop Translat. 2017;9:8–18.
15. Dowdell J, Erwin M, Choma T, Vaccaro A, Iatridis J, Cho SK. Intervertebral disk degeneration and repair. Neurosurgery. 2017;80(3s):S46-s54.
16. Kim M, Kim HS, Oh SW, Adsul NM, Singh R, Kashlan ON, et al. Evolution of spinal endoscopic surgery. Neurospine. 2019;16(1):6–14.
17. Buy X, Gangi A. Percutaneous treatment of intervertebral disc herniation. Semin Intervent Radiol. 2010;27(2):148–59.
18. Gerszten PC, Smuck M, Rathmell JP, Simopoulos TT, Bhagia SM, Mocek CK, et al. Plasma disc decompression compared with fluoroscopy-guided transforaminal epidural steroid injections for symptomatic contained lumbar disc herniation: a prospective, randomized, controlled trial. J Neurosurg Spine. 2010;12(4):357–71.
19. Kloppenburg M, Berenbaum F. Osteoarthritis year in review 2019: epidemiology and therapy. Osteoarthritis Cartilage. 2020;28(3):242–8.
20. Fritzell P, Hägg O, Wessberg P, Nordwall A. Volvo Award Winner in Clinical Studies: Lumbar fusion versus nonsurgical treatment for chronic low back pain: a multicenter randomized controlled trial from the Swedish Lumbar Spine Study Group. Spine (Phila Pa 1976). 2001;26(23):2521–32 (**discussion 32-4**).
21. Maroudas A, Stockwell RA, Nachemson A, Urban J. Factors involved in the nutrition of the human lumbar intervertebral disc: cellularity and diffusion of glucose in vitro. J Anat. 1975;120(Pt 1):113–30.
22. Trout JJ, Buckwalter JA, Moore KC. Ultrastructure of the human intervertebral disc: II. Cells of the nucleus pulposus. Anat Rec. 1982;204(4):307–14.
23. Chan WC, Sze KL, Samartzis D, Leung VY, Chan D. Structure and biology of the intervertebral disk in health and disease. Orthop Clin North Am. 2011;42(4):447–64, vii.
24. Yan P, Sun C, Luan L, Han J, Qu Y, Zhou C, et al. Hsa_circ_0134111 promotes intervertebral disc degeneration via sponging miR-578. Cell Death Discov. 2022;8(1):55.
25. Pei BQ, Li H, Zhu G, Li DY, Fan YB, Wu SQ. The application of fiber-reinforced materials in disc repair. Biomed Res Int. 2013;2013: 714103.
26. Newman HR, Bowles RD, Buckley MR. Viscoelastic heating of insulated bovine intervertebral disc. JOR Spine. 2018;1(1): e1002.
27. Hardin JA, Cobelli N, Santambrogio L. Consequences of metabolic and oxidative modifications of cartilage tissue. Nat Rev Rheumatol. 2015;11(9):521–9.
28. Hernandez PA, Jacobsen TD, Chahine NO. Actomyosin contractility confers mechanoprotection against TNFα-induced disruption of the intervertebral disc. Sci Adv. 2020;6(34):eaba2368.
29. Gan Y, He J, Zhu J, Xu Z, Wang Z, Yan J, et al. Spatially defined single-cell transcriptional profiling characterizes diverse chondrocyte subtypes and nucleus pulposus progenitors in human intervertebral discs. Bone Res. 2021;9(1):37.
30. Gruber HE, Ingram JA, Hoelscher GL, Zinchenko N, Hanley EN Jr, Sun Y. Asporin, a susceptibility gene in osteoarthritis, is expressed at higher levels in the more degenerate human intervertebral disc. Arthritis Res Ther. 2009;11(2):R47.
31. Gruber HE, Hoelscher GL, Ingram JA, Hanley EN Jr. Genome-wide analysis of pain-, nerve- and neurotrophin-related gene expression in the degenerating human annulus. Mol Pain. 2012;8:63.
32. Chen WT, Lu A, Craessaerts K, Pavie B, Sala Frigerio C, Corthout N, et al. Spatial transcriptomics and in situ sequencing to study Alzheimer's disease. Cell. 2020;182(4):976-91.e19.
33. Gautier L, Cope L, Bolstad BM, Irizarry RA. affy–analysis of affymetrix GeneChip data at the probe level. Bioinformatics. 2004;20(3):307–15.
34. Irizarry RA, Hobbs B, Collin F, Beazer-Barclay YD, Antonellis KJ, Scherf U, et al. Exploration, normalization, and summaries of high density oligonucleotide array probe level data. Biostatistics. 2003;4(2):249–64.
35. Leek JT, Johnson WE, Parker HS, Jaffe AE, Storey JD. The sva package for removing batch effects and other unwanted variation in high-throughput experiments. Bioinformatics. 2012;28(6):882–3.
36. Zhang X, Lan Y, Xu J, Quan F, Zhao E, Deng C, et al. Cell Marker: a manually curated resource of cell markers in human and mouse. Nucleic Acids Res. 2019;47(D1):D721–8.
37. Butler A, Hoffman P, Smibert P, Papalexi E, Satija R. Integrating single-cell transcriptomic data across different conditions, technologies, and species. Nat Biotechnol. 2018;36(5):411–20.
38. Wang Y, Wang R, Zhang S, Song S, Jiang C, Han G, et al. iTALK: an R package to characterize and illustrate intercellular communication. BioRxiv. 2019;18:507871.
39. Durinck S, Spellman PT, Birney E, Huber W. Mapping identifiers for the integration of genomic datasets with the R/Bioconductor package biomaRt. Nat Protoc. 2009;4(8):1184–91.
40. Qiu X, Mao Q, Tang Y, Wang L, Chawla R, Pliner HA, et al. Reversed graph embedding resolves complex single-cell trajectories. Nat Methods. 2017;14(10):979–82.
41. Ringnér M. What is principal component analysis? Nat Biotechnol. 2008;26(3):303–4.
42. Kirnaz S, Capadona C, Wong T, Goldberg JL, Medary B, Sommer F, et al. Fundamentals of intervertebral disc degeneration. World Neurosurg. 2022;157:264–73.
43. Thompson JP, Pearce RH, Schechter MT, Adams ME, Tsang IK, Bishop PB. Preliminary evaluation of a scheme for grading the gross morphology of the human intervertebral disc. Spine (Phila Pa 1976). 1990;15(5):411–5.
44. Pfirrmann CW, Metzdorf A, Zanetti M, Hodler J, Boos N. Magnetic resonance classification of lumbar intervertebral disc degeneration. Spine (Phila Pa 1976). 2001;26(17):1873–8.
45. Fei J, Liang B, Jiang C, Ni H, Wang L. Luteolin inhibits IL-1β-induced inflammation in rat chondrocytes and attenuates osteoarthritis progression in a rat model. Biomed Pharmacother. 2019;109:1586–92.
46. Ye J, Coulouris G, Zaretskaya I, Cutcutache I, Rozen S, Madden TL. Primer-BLAST: a tool to design target-specific primers for polymerase chain reaction. BMC Bioinformatics. 2012;13:134.
47. Ohba S, He X, Hojo H, McMahon AP. Distinct transcriptional programs underlie Sox9 regulation of the mammalian chondrocyte. Cell Rep. 2015;12(2):229–43.
48. Ng LJ, Wheatley S, Muscat GE, Conway-Campbell J, Bowles J, Wright E, et al. SOX9 binds DNA, activates transcription, and coexpresses with type II collagen during chondrogenesis in the mouse. Dev Biol. 1997;183(1):108–21.
49. Schwab W, Gavlik JM, Beichler T, Funk RH, Albrecht S, Magdolen V, et al. Expression of the urokinase-type plasminogen activator receptor in human articular chondrocytes: association with caveolin and beta 1-integrin. Histochem Cell Biol. 2001;115(4):317–23.
50. Loeser RF. Chondrocyte integrin expression and function. Biorheology. 2000;37(1–2):109–16.
51. Zhong H, Li M, Wu H, Ying H, Zhong M, Huang M. Silencing DDX3 attenuates interleukin-1β-induced intervertebral disc degeneration through inhibiting pyroptosis. Inflammation. 2024. https://doi.org/10.1007/s10753-024-02042-1.
52. Caliskan T, Sirin DY, Karaarslan N, Yilmaz I, Ozbek H, Akyuva Y, et al. Effects of etanercept, a tumor necrosis factor receptor fusion protein, on primary cell cultures prepared from intact human intervertebral disc tissue. Exp Ther Med. 2019;18(1):69–76.
53. Karaarslan N, Yilmaz I, Sirin DY, Ozbek H, Kaplan N, Kaya YE, et al. Pregabalin treatment for neuropathic pain may damage intervertebral disc tissue. Exp Ther Med. 2018;16(2):1259–65.
54. Rhee J, Ryu JH, Kim JH, Chun CH, Chun JS. α-Catenin inhibits β-catenin-T-cell factor/lymphoid enhancing factor transcriptional activity and collagen type II expression in articular chondrocytes through formation of Gli3R.α-catenin.β-catenin ternary complex. J Biol Chem. 2012;287(15):11751–60.
55. Karaarslan N, Yilmaz I, Ozbek H, Yasar Sirin D, Kaplan N, Caliskan T, et al. Are radio-contrast agents commonly used in discography toxic to the intact intervertebral disc tissue cells? Basic Clin Pharmacol Toxicol. 2019;124(2):181–9.
56. Karaarslan N, Batmaz AG, Yilmaz I, Ozbek H, Caliskan T, Yasar Sirin D, et al. Effect of naproxen on proliferation and differentiation of primary cell cultures isolated from human cartilage tissue. Exp Ther Med. 2018;16(3):1647–54.
57. Knudson CB, Knudson W. Hyaluronan-binding proteins in development, tissue homeostasis, and disease. Faseb j. 1993;7(13):1233–41.
58. Knudson W, Chow G, Knudson CB. CD44-mediated uptake and degradation of hyaluronan. Matrix Biol. 2002;21(1):15–23.

59. Geread RS, Morreale P, Dony RD, Brouwer E, Wood GA, Androutsos D, et al. IHC color histograms for unsupervised Ki67 proliferation index calculation. Front Bioeng Biotechnol. 2019;7:226.
60. Xue J, Yang W, Wang X, Wang P, Meng X, Yu T, et al. A transcriptome sequencing study on the effect of macro-pores in hydrogel scaffolds on global gene expression of laden human cartilage chondrocytes. Biomed Mater. 2022;17(4): 044102.
61. Miyamoto Y, Uga H, Tanaka S, Kadowaki M, Ikeda M, Saegusa J, et al. Podoplanin is an inflammatory protein upregulated in Th17 cells in SKG arthritic joints. Mol Immunol. 2013;54(2):199–207.
62. Ekwall AK, Eisler T, Anderberg C, Jin C, Karlsson N, Brisslert M, et al. The tumour-associated glycoprotein podoplanin is expressed in fibroblast-like synoviocytes of the hyperplastic synovial lining layer in rheumatoid arthritis. Arthritis Res Ther. 2011;13(2):R40.
63. Lai T, Cho H, Liu Z, Bowler MW, Piao S, Parker R, et al. Structural basis of the PNRC2-mediated link between mrna surveillance and decapping. Structure. 2012;20(12):2025–37.
64. Hummert TW, Schwartz Z, Sylvia VL, Dean DD, Hardin RR, Boyan BD. Expression and production of stathmin in growth plate chondrocytes is cell-maturation dependent. J Cell Biochem. 2000;79(1):150–63.
65. Lu Z, Wang D, Sun Y, Dai Y. ENO1 regulates IL-1β-induced chondrocyte inflammation, apoptosis and matrix degradation possibly through the potential binding to CRLF1. Tissue Cell. 2024;90: 102504.
66. Tsolis KC, Bei ES, Papathanasiou I, Kostopoulou F, Gkretsi V, Kalantzaki K, et al. Comparative proteomic analysis of hypertrophic chondrocytes in osteoarthritis. Clin Proteomics. 2015;12(1):12.
67. Cherif H, Mannarino M, Pacis AS, Ragoussis J, Rabau O, Ouellet JA, et al. Single-cell RNA-seq analysis of cells from degenerating and non-degenerating intervertebral discs from the same individual reveals new biomarkers for intervertebral disc degeneration. Int J Mol Sci. 2022;23(7):3993.
68. Melrose J, Guilak F. Diverse and multifunctional roles for perlecan (HSPG2) in repair of the intervertebral disc. JOR Spine. 2024;7(3): e1362.
69. Kazezian Z, Gawri R, Haglund L, Ouellet J, Mwale F, Tarrant F, et al. Gene expression profiling identifies interferon signalling molecules and IGFBP3 in human degenerative annulus fibrosus. Sci Rep. 2015;5:15662.
70. Easson GWD, Savadipour A, Anandarajah A, Iannucci LE, Lake SP, Guilak F, et al. Modulation of TRPV4 protects against degeneration induced by sustained loading and promotes matrix synthesis in the intervertebral disc. Faseb J. 2023;37(2): e22714.
71. Fernandes LM, Khan NM, Trochez CM, Duan M, Diaz-Hernandez ME, Presciutti SM, et al. Single-cell RNA-seq identifies unique transcriptional landscapes of human nucleus pulposus and annulus fibrosus cells. Sci Rep. 2020;10(1):15263.
72. Hu X, Wang Z, Zhang H, Cui P, Li Y, Chen X, et al. Single-cell sequencing: New insights for intervertebral disc degeneration. Biomed Pharmacother. 2023;165: 115224.
73. Hickman TT, Rathan-Kumar S, Peck SH. Development, pathogenesis, and regeneration of the intervertebral disc: current and future insights spanning traditional to omics methods. Front Cell Dev Biol. 2022;10: 841831.
74. Zhang Y, Han S, Kong M, Tu Q, Zhang L, Ma X. Single-cell RNA-seq analysis identifies unique chondrocyte subsets and reveals involvement of ferroptosis in human intervertebral disc degeneration. Osteoarthritis Cartilage. 2021;29(9):1324–34.
75. Han S, Zhang Y, Zhang X, Zhang H, Meng S, Kong M, et al. Single-Cell RNA sequencing of the nucleus pulposus reveals chondrocyte differentiation and regulation in intervertebral disc degeneration. Front Cell Dev Biol. 2022;10: 824771.
76. Li FC, Zhang N, Chen WS, Chen QX. Endplate degeneration may be the origination of the vacuum phenomenon in intervertebral discs. Med Hypotheses. 2010;75(2):169–71.
77. Baskozos G, Sandy-Hindmarch O, Clark AJ, Windsor K, Karlsson P, Weir GA, et al. Molecular and cellular correlates of human nerve regeneration: ADCYAP1/PACAP enhance nerve outgrowth. Brain. 2020;143(7):2009–26.
78. Reglodi D, Kiss P, Szabadfi K, Atlasz T, Gabriel R, Horvath G, et al. PACAP is an endogenous protective factor-insights from PACAP-deficient mice. J Mol Neurosci. 2012;48(3):482–92.
79. Reglodi D, Kiss P, Lubics A, Tamas A. Review on the protective effects of PACAP in models of neurodegenerative diseases in vitro and in vivo. Curr Pharm Des. 2011;17(10):962–72.
80. Abad C, Waschek JA. Immunomodulatory roles of VIP and PACAP in models of multiple sclerosis. Curr Pharm Des. 2011;17(10):1025–35.
81. Vaudry D, Falluel-Morel A, Bourgault S, Basille M, Burel D, Wurtz O, et al. Pituitary adenylate cyclase-activating polypeptide and its receptors: 20 years after the discovery. Pharmacol Rev. 2009;61(3):283–357.
82. Somogyvári-Vigh A, Reglodi D. Pituitary adenylate cyclase activating polypeptide: a potential neuroprotective peptide. Curr Pharm Des. 2004;10(23):2861–89.
83. Tsuchida M, Nakamachi T, Sugiyama K, Tsuchikawa D, Watanabe J, Hori M, et al. PACAP stimulates functional recovery after spinal cord injury through axonal regeneration. J Mol Neurosci. 2014;54(3):380–7.
84. Juhász T, Matta C, Katona É, Somogyi C, Takács R, Gergely P, et al. Pituitary adenylate cyclase activating polypeptide (PACAP) signalling exerts chondrogenesis promoting and protecting effects: implication of calcineurin as a downstream target. PLoS ONE. 2014;9(3): e91541.
85. Tsuchikawa D, Nakamachi T, Tsuchida M, Wada Y, Hori M, Farkas J, et al. Neuroprotective effect of endogenous pituitary adenylate cyclase-activating polypeptide on spinal cord injury. J Mol Neurosci. 2012;48(3):508–17.
86. Fang KM, Chen JK, Hung SC, Chen MC, Wu YT, Wu TJ, et al. Effects of combinatorial treatment with pituitary adenylate cyclase activating peptide and human mesenchymal stem cells on spinal cord tissue repair. PLoS ONE. 2010;5(12): e15299.
87. Sun BY, Sun ZP, Pang ZC, Huang WT, Wu SP. Decreased synovial fluid pituitary adenylate cyclase-activating polypeptide (PACAP) levels may reflect disease severity in post-traumatic knee osteoarthritis after anterior cruciate ligament injury. Peptides. 2019;116:22–9.
88. Reglodi D, Jungling A, Longuespée R, Kriegsmann J, Casadonte R, Kriegsmann M, et al. Accelerated pre-senile systemic amyloidosis in PACAP knockout mice—a protective role of PACAP in age-related degenerative processes. J Pathol. 2018;245(4):478–90.
89. Szentléleky E, Szegeczki V, Karanyicz E, Hajdú T, Tamás A, Tóth G, et al. Pituitary adenylate cyclase activating polypeptide (PACAP) reduces oxidative and mechanical stress-evoked matrix degradation in chondrifying cell cultures. Int J Mol Sci. 2019;20(1):168.
90. Philbrick WM, Wysolmerski JJ, Galbraith S, Holt E, Orloff JJ, Yang KH, et al. Defining the roles of parathyroid hormone-related protein in normal physiology. Physiol Rev. 1996;76(1):127–73.
91. Petersson M, Bucht E, Granberg B, Stark A. Effects of arginine-vasopressin and parathyroid hormone-related protein (1–34) on cell proliferation and production of YKL-40 in cultured chondrocytes from patients with rheumatoid arthritis and osteoarthritis. Osteoarthritis Cartilage. 2006;14(7):652–9.
92. Fischer J, Aulmann A, Dexheimer V, Grossner T, Richter W. Intermittent PTHrP(1–34) exposure augments chondrogenesis and reduces hypertrophy of mesenchymal stromal cells. Stem Cells Dev. 2014;23(20):2513–23.
93. Wang ST, Gao YJ, Duan CC, Li DD, Tian XC, Zhang QL, et al. Effects of PTHrP on expression of MMP9 and MMP13 in sika deer antler chondrocytes. Cell Biol Int. 2013;37(12):1300–7.
94. Weir EC, Philbrick WM, Amling M, Neff LA, Baron R, Broadus AE. Targeted overexpression of parathyroid hormone-related peptide in chondrocytes causes chondrodysplasia and delayed endochondral bone formation. Proc Natl Acad Sci USA. 1996;93(19):10240–5.
95. Karaplis AC, Luz A, Glowacki J, Bronson RT, Tybulewicz VL, Kronenberg HM, et al. Lethal skeletal dysplasia from targeted disruption of the parathyroid hormone-related peptide gene. Genes Dev. 1994;8(3):277–89.
96. Nishimori S, Lai F, Shiraishi M, Kobayashi T, Kozhemyakina E, Yao TP, et al. PTHrP targets HDAC4 and HDAC5 to repress chondrocyte hypertrophy. JCI Insight. 2019;4(5):e97903.
97. Duan ZX, Huang P, Tu C, Liu Q, Li SQ, Long ZL, et al. MicroRNA-15a-5p regulates the development of osteoarthritis by targeting PTHrP in chondrocytes. Biomed Res Int. 2019;2019:3904923.
98. Berg LC, Mata X, Thomsen PD. Molecular characterization and chromosomal assignment of equine cartilage derived retinoic acid sensitive protein (CD-RAP)/melanoma inhibitory activity (MIA). Gene. 2008;407(1–2):98–104.

99. Tscheudschilsuren G, Bosserhoff AK, Schlegel J, Vollmer D, Anton A, Alt V, et al. Regulation of mesenchymal stem cell and chondrocyte differentiation by MIA. Exp Cell Res. 2006;312(1):63–72.
100. Dietz UH, Sandell LJ. Cloning of a retinoic acid-sensitive mRNA expressed in cartilage and during chondrogenesis. J Biol Chem. 1996;271(6):3311–6.
101. Bosserhoff AK, Kondo S, Moser M, Dietz UH, Copeland NG, Gilbert DJ, et al. Mouse CD-RAP/MIA gene: structure, chromosomal localization, and expression in cartilage and chondrosarcoma. Dev Dyn. 1997;208(4):516–25.
102. Sakano S, Zhu Y, Sandell LJ. Cartilage-derived retinoic acid-sensitive protein and type II collagen expression during fracture healing are potential targets for Sox9 regulation. J Bone Miner Res. 1999;14(11):1891–901.
103. Müller-Ladner U, Bosserhoff AK, Dreher K, Hein R, Neidhart M, Gay S, et al. MIA (melanoma inhibitory activity): a potential serum marker for rheumatoid arthritis. Rheumatology (Oxford). 1999;38(2):148–54.
104. Neidhart M, Müller-Ladner U, Frey W, Bosserhoff AK, Colombani PC, Frey-Rindova P, et al. Increased serum levels of non-collagenous matrix proteins (cartilage oligomeric matrix protein and melanoma inhibitory activity) in marathon runners. Osteoarthritis Cartilage. 2000;8(3):222–9.
105. Bosserhoff AK, Buettner R. Establishing the protein MIA (melanoma inhibitory activity) as a marker for chondrocyte differentiation. Biomaterials. 2003;24(19):3229–34.
106. Vandooren B, Cantaert T, van Lierop MJ, Bos E, De Rycke L, Veys EM, et al. Melanoma inhibitory activity, a biomarker related to chondrocyte anabolism, is reversibly suppressed by proinflammatory cytokines in rheumatoid arthritis. Ann Rheum Dis. 2009;68(6):1044–50.
107. Chansky H, Robbins JR, Cha S, Raskind WH, Conrad EU, Sandell LJ. Expression of cartilage extracellular matrix and potential regulatory genes in a new human chondrosarcoma cell line. J Orthop Res. 1998;16(5):521–30.
108. Blesch A, Bosserhoff AK, Apfel R, Behl C, Hessdoerfer B, Schmitt A, et al. Cloning of a novel malignant melanoma-derived growth-regulatory protein. MIA Cancer Res. 1994;54(21):5695–701.
109. Yeremenko N, Härle P, Cantaert T, van Tok M, van Duivenvoorde LM, Bosserhoff A, et al. The cartilage protein melanoma inhibitory activity contributes to inflammatory arthritis. Rheumatology (Oxford). 2014;53(3):438–47.
110. Jordan MA, Wilson L. Microtubules as a target for anticancer drugs. Nat Rev Cancer. 2004;4(4):253–65.
111. Gilbertson-White S, Perkhounkova Y, Saeidzadeh S, Hein M, Dahl R, Simons-Burnett A. Understanding symptom burden in patients with advanced cancer living in rural areas. Oncol Nurs Forum. 2019;46(4):428–41.
112. Bates D, Eastman A. Microtubule destabilising agents: far more than just antimitotic anticancer drugs. Br J Clin Pharmacol. 2017;83(2):255–68.
113. Nami B, Wang Z. Genetics and expression profile of the tubulin gene superfamily in breast cancer subtypes and its relation to taxane resistance. Cancers (Basel). 2018;10(8):274.
114. Ilan Y. Microtubules: from understanding their dynamics to using them as potential therapeutic targets. J Cell Physiol. 2019;234(6):7923–37.
115. Zhu H, Hu X, Gu L, Jian Z, Li L, Hu S, et al. TUBA1C is a prognostic marker in low-grade glioma and correlates with immune cell infiltration in the tumor microenvironment. Front Genet. 2021;12: 759953.
116. Moiseeva EP, Williams B, Goodall AH, Samani NJ. Galectin-1 interacts with beta-1 subunit of integrin. Biochem Biophys Res Commun. 2003;310(3):1010–6.
117. Elola MT, Chiesa ME, Alberti AF, Mordoh J, Fink NE. Galectin-1 receptors in different cell types. J Biomed Sci. 2005;12(1):13–29.
118. Camby I, Le Mercier M, Lefranc F, Kiss R. Galectin-1: a small protein with major functions. Glycobiology. 2006;16(11):137r-r157.
119. Baum LG, Blackall DP, Arias-Magallano S, Nanigian D, Uh SY, Browne JM, et al. Amelioration of graft versus host disease by galectin-1. Clin Immunol. 2003;109(3):295–307.
120. Liu SD, Lee S, La Cava A, Motran CC, Hahn BH, Miceli MC. Galectin-1-induced down-regulation of T lymphocyte activation protects (NZB x NZW) F1 mice from lupus-like disease. Lupus. 2011;20(5):473–84.
121. Rabinovich GA, Daly G, Dreja H, Tailor H, Riera CM, Hirabayashi J, et al. Recombinant galectin-1 and its genetic delivery suppress collagen-induced arthritis via T cell apoptosis. J Exp Med. 1999;190(3):385–98.
122. Marcon P, Marsich E, Vetere A, Mozetic P, Campa C, Donati I, et al. The role of Galectin-1 in the interaction between chondrocytes and a lactose-modified chitosan. Biomaterials. 2005;26(24):4975–84.
123. Toegel S, Weinmann D, André S, Walzer SM, Bilban M, Schmidt S, et al. Galectin-1 couples glycobiology to inflammation in osteoarthritis through the activation of an NF-κB-regulated gene network. J Immunol. 2016;196(4):1910–21.
124. Ye X, Sun M. AGR2 ameliorates tumor necrosis factor-α-induced epithelial barrier dysfunction via suppression of NF-κB p65-mediated MLCK/p-MLC pathway activation. Int J Mol Med. 2017;39(5):1206–14.
125. Singh JA, Arayssi T, Duray P, Schumacher HR. Immunohistochemistry of normal human knee synovium: a quantitative study. Ann Rheum Dis. 2004;63(7):785–90.
126. Potlog-Nahari C, Feldman AL, Stratton P, Koziol DE, Segars J, Merino MJ, et al. CD10 immunohistochemical staining enhances the histological detection of endometriosis. Fertil Steril. 2004;82(1):86–92.
127. Rowan DJ, Mangalaparthi KK, Singh S, Moreira RK, Mounajjed T, Lamps L, et al. Metallothionein immunohistochemistry has high sensitivity and specificity for detection of Wilson disease. Mod Pathol. 2022;35(7):946–55.
128. Nasr SH, Fogo AB. New developments in the diagnosis of fibrillary glomerulonephritis. Kidney Int. 2019;96(3):581–92.
129. Geeleher P, Cox N, Huang RS. pRRophetic: an R package for prediction of clinical chemotherapeutic response from tumor gene expression levels. PLoS ONE. 2014;9(9): e107468.
130. Geeleher P, Cox NJ, Huang RS. Clinical drug response can be predicted using baseline gene expression levels and in vitro drug sensitivity in cell lines. Genome Biol. 2014;15(3):R47.
131. Garnett MJ, Edelman EJ, Heidorn SJ, Greenman CD, Dastur A, Lau KW, et al. Systematic identification of genomic markers of drug sensitivity in cancer cells. Nature. 2012;483(7391):570–5.
132. Wang Z, Wang Y, Yang T, Xing H, Wang Y, Gao L, et al. Machine learning revealed stemness features and a novel stemness-based classification with appealing implications in discriminating the prognosis, immunotherapy and temozolomide responses of 906 glioblastoma patients. Brief Bioinform. 2021;22(5):bbab032.
133. Guo G, Wang Y, Kou W, Gan H. Identifying the molecular mechanisms of sepsis-associated acute kidney injury and predicting potential drugs. Front Genet. 2022;13:1062293.
134. Sun H, Wu Y, Pan Z, Yu D, Chen P, Zhang X, et al. Gefitinib for epidermal growth factor receptor activated osteoarthritis subpopulation treatment. EBioMedicine. 2018;32:223–33.
135. Zhang YW, Su Y, Lanning N, Swiatek PJ, Bronson RT, Sigler R, et al. Targeted disruption of Mig-6 in the mouse genome leads to early onset degenerative joint disease. Proc Natl Acad Sci USA. 2005;102(33):11740–5.
136. Appleton CT, Usmani SE, Bernier SM, Aigner T, Beier F. Transforming growth factor alpha suppression of articular chondrocyte phenotype and Sox9 expression in a rat model of osteoarthritis. Arthritis Rheum. 2007;56(11):3693–705.
137. Appleton CT, Usmani SE, Mort JS, Beier F. Rho/ROCK and MEK/ERK activation by transforming growth factor-alpha induces articular cartilage degradation. Lab Invest. 2010;90(1):20–30.
138. Appleton CT, Usmani SE, Pest MA, Pitelka V, Mort JS, Beier F. Reduction in disease progression by inhibition of transforming growth factor α-CCL2 signaling in experimental posttraumatic osteoarthritis. Arthritis Rheumatol. 2015;67(10):2691–701.
139. Usmani SE, Ulici V, Pest MA, Hill TL, Welch ID, Beier F. Context-specific protection of TGFα null mice from osteoarthritis. Sci Rep. 2016;6:30434.
140. Appleton CT, Pitelka V, Henry J, Beier F. Global analyses of gene expression in early experimental osteoarthritis. Arthritis Rheum. 2007;56(6):1854–68.
141. Pan Z, Wu Y, Zhang X, Fu Q, Li J, Yang Y, et al. Delivery of epidermal growth factor receptor inhibitor via a customized collagen scaffold promotes meniscal defect regeneration in a rabbit model. Acta Biomater. 2017;62:210–21.
142. Pan Z, Sun H, Xie B, Xia D, Zhang X, Yu D, et al. Therapeutic effects of gefitinib-encapsulated thermosensitive injectable hydrogel in intervertebral disc degeneration. Biomaterials. 2018;160:56–68.
143. Moryl N, Obbens EA, Ozigbo OH, Kris MG. Analgesic effect of gefitinib in the treatment of non-small cell lung cancer. J Support Oncol. 2006;4(3):111.
144. Zhang X, Zhu J, Liu F, Li Y, Chandra A, Levin LS, et al. Reduced EGFR signaling enhances cartilage destruction in a mouse osteoarthritis model. Bone Res. 2014;2:14015.